Zircon U-Pb geochronology and Hf isotopes of the Luís Alves Terrane: Archean to Paleoproterozoic evolution and Neoproterozoic overprint

Beatrix M. Heller, Mathias Hueck, Claudia R. Passarelli, Miguel A.A. Basei

Journal Pre-proof

Zircon U-Pb geochronology and Hf isotopes of the Luís Alves Terrane: Archean to Paleoproterozoic evolution and Neoproterozoic overprint

Beatrix M. Heller, Mathias Hueck, Claudia R. Passarelli, Miguel A.S. Basei

PII: S0895-9811(20)30551-4

DOI: https://doi.org/10.1016/j.jsames.2020.103008

Reference: SAMES 103008

To appear in: *Journal of South American Earth Sciences*

Received Date: 7 August 2020

Revised Date: 31 October 2020

Accepted Date: 2 November 2020

Please cite this article as: Heller, B.M., Hueck, M., Passarelli, C.R., Basei, M.A.S., Zircon U-Pb geochronology and Hf isotopes of the Luís Alves Terrane: Archean to Paleoproterozoic evolution and Neoproterozoic overprint, *Journal of South American Earth Sciences* (2020), doi: https://doi.org/10.1016/j.jsames.2020.103008.

Zircon U-Pb geochronology and Hf isotopes of the Luís Alves Terrane: Archean to Paleoproterozoic evolution and Neoproterozoic overprint

Beatrix M. Heller[1,2], Mathias Hueck[1], Claudia R. Passarelli[1], Miguel A. S. Basei[1]

[1]Instituto de Geociências, Universidade de São Paulo, São Paulo, Brazil

[2]Université Paris-Saclay, CNRS, GEOPS, 91405, Orsay, France

Abstract

The Luís Alves Terrane in southern Brazil is one of the largest expositions of the Archean to Paleoproterozoic units that acted as basement for the development of the Neoproterozoic Pan-African/Brasiliano orogenic belts in the Mantiqueira Province, in South America. Combined field observations, petrography, Hf and U-Pb LA-ICP-MS zircon and titanite isotopic data are presented for the basement of this terrane. The zircon U-Pb dataset spans a large time range with concordant ages from 3.2-1.8 Ga. Several magmatic and metamorphic events are recorded by the U-Pb concordant ages reflecting the complex evolution of this crustal block. The oldest inherited zircon grains have Mesoarchean ages (3.2-3.1 Ga), while two other magmatic populations yield ages of 2,683±70 Ma and 2,498±11 Ma. Most zircon grains crystallized during two high-grade metamorphic events at 2,352±23 Ma and 2,183±17 Ma. Titanite from two samples crystallized at 2.02-1.99 Ga, probably during a retrograde metamorphic trajectory that re-equilibrated the studied samples in amphibolite-facies conditions. A late pegmatite dyke was emplaced between ca. 1.96 and 1.79 Ga. Cathodoluminescence images show that the analyzed zircon samples, including those in the pegmatite, had their internal structure modified by hydrothermal processes. The localization of the outcrop close to the rim of the Campo Alegre Basin affected by an important Neoproterozoic hydrothermal event as well as normal and reverse discordant U-Pb ages in our dataset indicate that this event took place during the Brasiliano orogenic cycle at the end of the Neoproterozoic. The Hf isotope data show predominantly crustal signatures with εHf(t) values ranging from 1.3 to -16.8. Hf T_{DM} model ages cluster in two groups (4.32-3.48 and 3.38-2.27 Ga) indicating two pulses of magma differentiation from the mantle with subsequent mixing of the material during the Paleoproterozoic high grade metamorphic events.

Keywords: Luís Alves Terrane, U-Pb geochronology, Zircon Lu-Hf isotopy, hydrothermal zircon.

1. Introduction

Zircon crystals from granulitic terranes commonly have complex textures recording multiple crystallization events that can be associated to both magmatism and high-grade metamorphism (Corfu 2003; Hoskin and Black 2000; Kröner et al. 2014; Zhao et al. 2015; Oriolo et al. 2016). A common consequence in HT to UHT terranes is the expanded spreading of U-Pb zircon data along the Concordia or bordering a sub-parallel Discordia line whose meaning requires careful interpretation. The spread of zircon ages may be attributed to a sequence of metamorphic events with episodic zircon growth or partial resetting (Whitehouse and Kemp 2010; Taylor et al. 2016; Rubatto 2017; Laurent et al. 2018; Tedeschi et al. 2018). Additionally, the implications for U-Pb geochronology are amplified in ancient geological terranes, in which the metamictization of zircon crystals results in a higher susceptibility to hydrothermal processes (Geisler et al. 2001). In this context, late opening of the isotopic system may result in complex datasets involving both normal and reverse discordance (Williams et al. 1984; Corfu 2013; Kusiak et al. 2013; Wiemer et al. 2017).

The Luis Alves Terrane (LAT), which is ca. 230km long and 50km wide is located in southern Brazil and is surrounded by orogenic belts formed during the Brasiliano / Panafrican orogenic cycle at the end of the Neoproterozoic and Cambrian (Basei et al. 1998a, 2009a, b; Passarelli et al. 2018; Siegesmund et al. 2018). Nonetheless, Neoproterozoic-Cambrian activity in the LAT was restricted to the emplacement of intrusive rocks (Kaul 1984; Gualda and Vlach 2007 a,b) and the development of (volcano-) sedimentary basins (Basei et al 1998b; Rostirolla et al. 1999; Citroni et al. 2001; Guadagnin et al. 2010; Basei et al. 2011b; Quiroz-Valle et al. 2019) while the crystalline basement, the Santa Catarina Granulitic Complex (SCGC), remained largely unaffected (Hartmann et al. 1979, 2000; Basei et al. 1992, 1998a; 2009b, Siga Jr. 1995; Harara et al., 2003; Passarelli et al 2018). All high-temperature geochronological data of the SCGC yield Paleoproterozoic and Archean ages (Basei 1985; Siga Jr 1995; Hartmann et al. 2000; Harara 2001; Basei et al 2009 a,b) and the only signs of reactivation of the basement during the Brasiliano orogenic cycle are ~ 600 Ma old K-Ar ages in shear zones (Siga Jr 1995).

In this study we present U-Pb LA-ICP-MS ages from zircon and titanite from one basement outcrop in the central-western portion of the LAT. Our data provide the required complement to the available geochronological data set which was mainly obtained from multi-crystal ID-TIMS zircon U-Pb ages and imprecise Rb-Sr whole rock ages .The new data confirm the suggested geochronological evolution and provide more precise age constraints for the main magmatic and metamorphic events that formed the LAT. Detailed evaluation of this complex dataset allows the recognition of a partial opening of the U-Pb system, probably during an hydrothermal event in the late Neoproterozoic Brasiliano orogenic cycle. This event led to redistribution of radiogenic Pb within and out of zircon crystals, resulting in a high number of normal and reverse discordant U-Pb ages. Furthermore, we present Hf isotope data for the LAT, which indicate that the LAT is composed of old crustal material extracted from the mantle in two main pulses which became progressively mixed during tectonic reworking in the Paleoproterozoic.

2. Geological setting

Southern Brazil is structurally marked by the juxtaposition of several geotectonic domains with different evolutions (Fig. 1). Neoproterozoic subduction and collision events led to the formation of Western Gondwana during the Brasiliano/Pan-African orogenic cycle affecting the crustal blocks to differing degrees (Heilbron et al. 2004; Basei et al. 2010; Passarelli et al. 2011; Oriolo et al. 2017; Siegesmund et al. 2018). The oldest domains are the Rio de la Plata and Paranapanema cratons, located to the west and presently mostly covered by the sediments of the Paraná Basin. The eastern border of these cratons are marked by two low- to medium-grade metamorphic metavolcano–sedimentary complexes and intrusive granitoids: the Ribeira Belt in the north and the Dom Feliciano Belt in the south. These tectonic domains are separated by two granite-gneiss terranes: the Curitiba Terrane, strongly migmatized in the Brasiliano orogenic cycle and the Luis Alves Terrane (LAT).

The Curitiba Terrane is located immediately to the South of the Ribeira Belt, separated by the Lancinha-Cubatão-Itariri Shear Zone (Passarelli et al. 2011). The crystalline basement is 60 km wide and 200 km long and contains the Atuba-Registro-Itatins Complex (Fig. 1). The basement is composed of banded migmatitic gneisses of Paleoproterozoic age (2.1–2.0 Ga) (Siga Jr 1995; Basei et al 1998a) that underwent intense deformation and migmatization during the Neoproterozoic. Features from a second Neoproterozoic migmatization phase occur commonly, associated with the Brasiliano/Pan-African orogenic cycle. The complex is partly covered by low-grade Neoproterozoic metavolcano-sedimentary sequences and was intruded by anorogenic alkaline–peralkaline granitoids of the late Neoproterozoic Serra do Mar Suite, commonly included in the alkaline Graciosa Province (Gualda and

Vlach 2007a,b; Vlach et al. 2011). The contact between the Curitiba Terrane and the LAT is made up of calc-alkaline granitoids of the Rio Piên Batholith as well as rocks of the Piên mafic ultramafic suite, both of which were heterogeneously deformed along the Piên and Mandirituba-Piraquara Shear Zone (Machiavelli et al. 1993; Harara 1996). The association is interpreted as remains of a dismembered ophiolitic complex (Basei et al. 1992; Machiavelli et al. 1993; Harara 2001).

The LAT is limited to the south by the Itajaí-Perimbó Shear Zone, which separates it from the Brusque Group and the Itajaí Basin, domains of the Dom Feliciano Belt (Fig. 1), which extends for over 1,400 km until Uruguay and was formed in the Neoproterozoic by the tectonic interaction between the Río de la Plata, Congo and Kalahari Cratons (Basei et al. 2000; Oyhantçabal et al. 2009; Philipp et al. 2016; Oriolo et al. 2016; Hueck et al. 2018). The Brusque Group is a poly-deformed metavolcano-sedimentary sequence that reached upper greenschist to lower amphibolite metamorphic facies (Philipp et al. 2004; Basei et al. 2011a, 2020) and was intruded at ca. 600 ± 15 Ma by voluminous granitic magmatism (Florisbal et al. 2012a, b; Hueck et al. 2016, 2020). Its crystalline basement is exposed in the Camboriú Complex, an association of gneiss-migmatitic rocks and granitic intrusions strongly reworked in the Brasiliano/Pan-African orogenic cycle (Bitencourt and Nardi 2004; Basei et al. 2013; Martini et al. 2015, 2019).

Lastly, the eastern termination of the Luís Alves Craton is the Costal Terrane,represented by the Paranaguá Domain. This igneous domain of Neoproterozoic origin (616-590 Ma) comprises a great variety of granitic rocks, most of them with calc-alkaline, magmatic arc signature. Metamorphic rocks such as gneisses, mica-schists quartzites and amphibolites occur as roof pendants within these granitoids (Basei et al. 1990; Siga Jr. 1995; Passarelli et al. 2004; Cury et al. 2008).

2.1. The Luis Alves Terrane

The LAT (Hartmann et al. 1979, 1998, 2000; Basei et al. 1992,1998a, 2009b; Siga Jr. 1995; Harara et al. 2002, 2003; Passarelli et al. 2018) consists of an Paleoproterozoic association with Archean protholiths, which in the Neoproterozoic was intruded by granites and locally covered by metavolcano-sedimentary basins. The basement units are grouped into the Santa Catarina Granulitic Complex (SCGC), predominantly a migmatitic–granitic–gneissic association with TTG signatures, while subordinately mafic and metasedimentary units also occur.

The southern portion of the LAT is dominated by biotite-amphibole gneiss with biotite-bearing mesosome and pink leucosome. Porphyritic biotite granites and pink mylonitic leucogranites are also common. More seldom are charnockitic–enderbitic rocks and lenticular meta–gabbro bodies in the gneisses forming strongly foliated amphibolites. The main structure is the gneissic foliation with an average orientation is of N30°E/51°NW. The central part of the terrane is dominated by grey charnockitic–enderbitic coarse–grained gneisses with a marked gneissic foliation and numerous enclaves and boudins of amphibolitic mafic rocks. Opx–bearing pegmatite veins cross-cut the gneissic foliation, which may indicate that the thermal apex postdated the main deformational event. Along the South Atlantic coast in the eastern portion of the LAT, the Barra Velha mafic–ultramafic Complex is boudinaged in the felsic granulitic gneisses and contains gabbro, gabbro–norite, amphibolite and websterite, thoroughly recrystallized by high–grade metamorphism (Minioli 1972; Fornari 1998).The northwestern region is dominated by greenish–grey amphibole–biotite–rich orthogneisses containing relicts of orthopyroxene, as well as mafic granulites with associated charnockitic-enderbitic portions. Lenses of amphibolitic schists, serpentinites, garnet–rich amphibolites, amphibolitic gneisses and felsic granulites occur locally. The predominant trend of the structures is NW–SE. In the northernmost portion of the LAT, leucocratic felsic tonalitic to granodioritic gneisses with many intercalations of greenish charnockite layers prevail, commonly with mylonitic portions.

Hyperstene in the orthogneisses indicates that the complex reached granulite facies. Even rocks without hyperstene show evidence of high grade metamorphism, such as brown biotite, antiperthitic sodic plagioclase and polygonized textures. Peak temperatures were estimated to 800° (Hartmann 1979, 2000) and the pressure to 5–7 kbar (Girardi and Ulbrich 1978; Fornari 1998). This high-grade event was followed by an amphibolite facies retrograde metamorphism and later, greenschist facies mineral assemblages formed along shear zones (Silva 1984; Basei 1985; Basei et al. 1998a). In its southernmost portion, along the Itajaí-Perimbó Shear Zone, highly deformed and reworked portions of the LAT are referred to as São Miguel Complex (Basei 1985). Zircon U-Pb SHRIMP age of tonalite from this complex is 2201± 7 Ma (Silva et al., 2000).

Available U-Pb, Rb-Sr, Sm-Nd and K-Ar geochronological data (Hartmann et al. 1979, 1998, 2000; Girardi et al 1974;Basei 1985;Basei et al. 1998a, 1999, 2000, 2009 a,b; Siga Jr 1995; Harara 2001; Sato et al. 2008, Passarelli et al. 2018) indicate an Archean to Paleoproterozoic evolution of the basement of the LAT with tectonic stabilization at the end of the Paleoproterozoic. However, most existing radiometric zircon ages were obtained by TIMS analyses and might partly result from mixed age populations. The oldest zircon U-Pb ages fall in the range of 2.7-2.6 Ga (SHRIMP, Hartmann et al 2000), Rb-Sr and Sm-Nd whole rock analyses yield similar results (Siga Jr 1995). These ages suggest Archean protoliths for the SCGC, even though the rocks were intensely overprinted by high-grade Paleoproterozoic metamorphism. Radiometric ages around 2.35 Ga can be found throughout the SCGC and are attributed to a high grade metamorphic event (Siga Jr 1995; Basei et al. 1998a, 1999, 2000, 2009b). U-Pb ages of 2.18 Ga in granulitic paragneisses indicate a second high grade metamorphic event, which apparently took place after a period of erosion and deposition of sedimentary rocks (Basei et al. 1998a, 1999, 2009b). Harara (2001) reports U-Pb ages (TIMS-ID) of 2.06 Ga which the author interprets as high grade metamorphic event. Sm-Nd TDM model ages are mainly Neoarchean and Siderian in age with individual ages being slightly older or younger (Harara 2001; Siga Jr 1995). K-Ar ages which mark the period of tectonic stabilization range from 2.1 to 1.7 Ga with a main peak for biotite at ca. 1.8 Ga (Girardi et al. 1974; Hartmann et al. 1979; Machiavelli 1991; Siga Jr 1995; Harara 2001). Younger K-Ar ages and one monazite U-Pb age of ~0.6 Ga were found near shear zones (Basei 1985, Siga Jr 1995).

The LAT was affected in the Neoproterozoic by localized granitic magmatism and the development of a set of volcano-sedimentary basins. The Serra do Mar Suite (Kaul 1984), alternatively named Graciosa Province (Gualda and Vlach 2007a,b), consists of A-type alkaline–peralkaline granitoid bodies which stretch parallel to the modern coastline. They are instrusive into the gneissic migmatitic basement and commonly carry xenoliths of gneissic rocks (Basei et al. 1990; Kaul 1997; Siga Jr et al. 1997, 1999). Geophysical, structural and textural characteristics as well as the correlation to the volcano–sedimentary basins indicate an emplacement at shallow crustal levels (Hallinan et al. 1993; Gualda and Vlach 2007a,b). The emplacement of the Serra do Mar Suite was at about 580-583 ±3 Ma, extensional A-type magmatism occurred ca. 10-30 Ma later, after the final amalgamation of the LAT, Curitiba and Paranaguá terranes (Vlach et al. 2011).

Along the northern portion of the LAT, the Campo Alegre, Corupá and Guaratubinha basins share similar lithological associations, and are therefore considered remnants of the same volcanosedimentary cover (Basei et al. 1998b). They mostly comprise terrigenous sediments covered by thick pyroclastic and volcanic sequences (Citroni et al. 2001; Quiroz-Valle et al. 2019), the onset of deposition of the lowermost unit of the Campo Alegre was constrained to ~606-590 Ma (Quiroz-Valle et al. 2019). Together with the A-type magmatism of the Serra do Mar Suite, these basins represent an important extensional phase after in the final stages of the Brasiliano/Pan-African orogenic cycle (Campos Neto and Figueiredo 1995; Campos Neto 2000; Almeida et al. 2010).

The other major Neoproterozoic sequence overlying the LAT is the Itajaí Basin (Rostirolla et al. 1999; Guadagnin et al. 2010; Basei et al. 2011b; Costa and Nascimento 2015), which covers much of the southern portion of the terrane. It is an elongated asymmetrical basin, with a total thickness that may add up to 5 km (Basei 1985; Basei et al. 1998b). The sedimentary sequence records basal polymitic conglomerates and massive sandstones, overlain by turbiditic rhythmites and immature sandstones and capped by silty-argillitic and silty-sandy sediments (Rostirolla et al. 1999; Guadagnin et al. 2010; Basei et al. 2011b; Costa and Nascimento 2015). Sedimentation began at ca. 595 Ma and ended by 560-550 Ma with the intrusion of rhyolitic dikes and domes in the upper sequences (Guadagnin et al. 2010; Basei et al. 2011b). New LA-ICP-MS U-Pb zircon data establish a minimum depositional age of 563±3 Ma and the Ediacaran fossil record indicates that the Itajaí Basin contains one of the oldest records of the Ediacaran biota in Gondwana (Becker-Kerber et al. 2020). The basin was affected by two deformation phases, causing local folding and numerous repetitions, and was intruded by the late Subida Granite at ca. 520 Ma (Basei et al.2008, 2011b).

3. Analyzed samples

In order to expand our understanding of the evolution of the Paleoproterozoic crust of the LAT, a lithologically complex outcrop, representative of the metamorphic units of the central exposures of the terrane, was chosen for detailed geochronological analyses. The outcrop is a ca. 10 m long and 2.5 m high roadcut close to São Bento do Sul (Fig. 1), along the highway that connects it to the town of Corupá (BR-280, coordinates: 26°17'57"S/ 49°23'52"W datum: WGS-84). The predominant lithology of the outcrop is banded gneisses with a strong foliation marked by a 10 to 30 cm thick banding (average attitude N090°/70°S) with tight isoclinal folds (Fig. 2A and B). A ca. 25 cm thick almond-shaped amphibolite boudin is hosted in gneiss in the northern portion of the outcrop (Fig. 2C), while in the southern portion there is a ca. 35 cm thick pegmatite dyke parallel to the banding (Fig. 2D). Four samples representing all lithologies were selected for U-Pb geochronology and Hf zircon isotopic analysis.

3.1. Orthogneiss (Samples TRX-04B and TRX-04C)

The predominant unit of the outcrop is a relatively homogeneous banded orthogneiss with a well-defined and continuous banding (Fig. 2B). Slight variations in the mineralogical composition occur between different bands, possibly suggesting some degree of magmatic heterogeneity in the protolith. Two samples were selected reflecting this discrete variety. *Sample TRX-04B* (Fig. 3A-B) represents a light grey fine- to medium-grained felsic band with syenogranitic composition. The rock typically has a granoblastic texture in which crystals have polygonal borders indicative of static crystallization. Mafic minerals include amphibole and biotite and are restricted to very thin layers that comprise less than 5% of the rock. Note that, in spite of the expected regional granulite facies context, no pyroxene is present in the sample and the gneiss has an equilibrated amphibolite-facies paragenesis. Accessory minerals include titanite, zircon and opaque minerals, as well as chlorite, epidote and calcite, which are indicative of retrometamorphism. This process is also suggested by the intense alteration of feldspars by means of sericitic and saussuritic transformations.

Sample TRX-04C, on the other hand, represents a more mafic band of the orthogneiss (Fig. 3C). The rock is a dark grey fine-grained gneiss with quartz-monzonitic composition. Foliation is defined by the alignment of amphiboles and biotites characterizing a nemato-lepidoblastic texture with mostly sutured crystal boundaries. Amphiboles are xeno- to subidioblastic and have strong pleocroism varying from pale yellowish-green to bluish-green. Titanite and zircon are accessory minerals, and

later hydrothermal alteration is suggested by the presence of epidote and chlorite, as well as by the alteration of feldspars.

3.2. Amphibolite (Sample TRX-04D)

The boudin-shaped amphibolite lens in the northern portion of the outcrop is represented by *SampleTRX-04D* (Fig. 3E-G). Foliation in this rock is less defined than in the orthogneiss, and is mostly characterized by the alignment of mafic mineral aggregates, which compose up to 30 % of the rock. The main minerals are plagioclase (ca. 60%) and amphibole (ca. 20%), with subordinate epidote and biotite. Amphiboles in thin section are very similar to those observed in the orthogneiss, and the rock has sutured crystal boundaries. Chlorite, calcite and the intense alteration of plagioclase indicate late retrometamorphism. Considerable amounts of epidote (up to 10%) may also be related to this event, or could be representative of the main metamorphic paragenesis, due to its elevated quantity and apparent equilibrium with biotite.

3.3. Pegmatite (Sample TRX-04A)

Lastly, *Sample TRX-04A* (Figs. 2D and 3H) represents the pegmatitic dyke in the southern portion of the outcrop. The dyke is parallel to the banding and foliation of the outcrop and the contact shows some softening of the surrounding orthogneiss, but it has no visible foliation and has an igneous texture. The pegmatite is salmon-colored and is dominated by very coarse grained feldspar crystals of several centimeters. As with the remaining rocks of the outcrop, the pegmatite was affected by later hydrothermalism, as indicated by intense sericitic and saussuritic transformation in feldspar and epidote-filled veins.

4. Results and mineralogical discussion

4.1. U-Pb geochronology

All U-Pb measurements were performed using the LA-MC-ICP-MS technique, following procedures detailed in Electronic Supplement S1. Concordia plots and weighted average ages calculated during interpretation of the dataset were performed using Isoplot/Ex 3.7 (Ludwig 2001). In total, 199 spot analyses were performed in zircon, however, 57 of them needed to be rejected due to high common lead contents or unrealistic concentrations after data reduction. In titanite, 65 spot analyses where performed yielding quite well constrained results and only two analyses needed to be rejected due to the same reasons. The high number of analyses with analytical difficulties and the difference observed in the overall consistency of the U-Pb dataset for titanite and zircon are probably a result of intensive hydrothermal alteration affecting both minerals differently. Spots that yielded results with analytical problems were discarded and were not considered during the interpretation of the U-Pb dataset. All remaining analyses, including both concordant and discordant results, are presented in the Electronic Supplements S2 and S3 organized according to the interpretation of each spot analysis. Because most of the concordant results yield Paleoproterozoic to Archean ages, whenever individual ages are mentioned they correspond to $^{207}Pb/^{206}Pb$ ages, except if noted otherwise.

4.1.1. Titanite results

Titanite U-Pb results are discussed first in this section because they are much more uniform than those of zircon, providing a rather straightforward interpretation that can be used as a geological constraint for interpreting the rest of the dataset. All results can be found in the Electronic Supplement S2.

A total of 33 spot analyses were performed in crystal fragments of sample *TRX-04C* (mafic orthogneiss). Analyzed crystals have common Pb contents mostly between 4 and 20%, and isotopic results are uniform with concordant single-spot ages between 2.05 and 1.96 Ga. A mean $^{207}Pb/^{206}Pb$ age of 1.991 ± 0.021 Ga was calculated considering all 33 spots (Fig. 4).

Results from sample *TRX-04D* (amphibolite) also have common Pb values up to 20%, but yielded more scattered isotopic ratios. A mean $^{207}Pb/^{206}Pb$ age of 2.027 ± 0.028 Ga was calculated using 28 of the 30 measured spots rejecting two outlying analyses (Fig. 4).

Both samples produced quite similar ages that are overlapping within uncertainty, resulting in a confident constraint of the timing of titanite crystallization in the studied lithological association at ca. 2.02-1.99 Ga. As will be discussed in Section 4.1.2., this particular time interval is notably absent in the dated zircon crystals from all rocks that have a penetrative metamorphic foliation. This suggest that the crystallization event recorded in the titanites took place under metamorphic conditions in which no new zircon crystals were crystallized and that promoted no overgrowth of metamorphic zircon. Hence, this event could be associated with the amphibolite-facies re-equilibration observed in all analyzed metamorphic rocks, presumably responsible for the substitution of the granulite-facies orthopyroxenes described in most occurrences of the Santa Catarina Granulitic Complex. This is in accordance with the fact that titanite in metabasic rocks is more stable in amphibolite facies than in granulite facies, where it is usually substituted by rutile or ilmenite (Frost et al. 2001; Kohn 2017). This interpretation is coherent with the geochronological evolution suggested for the rest of the dataset, but challenges previous mineralogical and geochemical observations that assumed a magmatic origin for titanite in syenitic rocks of the LAT (Hartmann et al. 1998).

4.1.2. Zircon results

Zircon crystals from all four samples show many different textures in cathodoluminescence imaging, some of which are rather complex and chaotic (Fig. 5A). Several grains contain textures typical for high grade metamorphism such as irregular concentric zoning, recrystallization in parts of the crystal or flow structures (Corfu et al. 2003; Taylor et al. 2016), examples are presented in Fig. 5A. All four analyzed samples show a similar transformation pattern which is exposed in the CL–images. The transformation is visible in form of so called spongy or porous textures (for simplicity only referred to as spongy in the following) (Fig. 5A). The samples are affected to different degrees, with the strongest modification seen in the pegmatite, which is the youngest sample of the outcrop and shows the most idiomorphic grains. In Corfu et al. (2003) and Nasdala et al. (2010) such spongy textures are described as a result of hydrothermal alteration. A more detailed discussion of this topic follows further down.

The transformation complicates the U–Pb analysis and the data interpretation. The loss of previous textural information inhibits a discrimination of the different parts of the zircons, and hydrothermal processes may lead to heterogeneous chemical distributions in crystals (e.g. Geisler et al. 2003; Anderson et al. 2008). In addition to the textural problems, the zircons of all four samples have many fractures and the possibilities of good spot locations are limited. In contrast to the titanite results, the U-Pb dataset obtained from zircon is characterized by a high number of discordant analyses with more than one third of the analyses being >10% discordant, many of which exhibit reverse discordance (Figs. 6 and 7). All results can be found in the electronic Supplement S3. Relating the quality of the analyses (including the rejected spots) to the textures (see Fig. 6) shows that the proportion of problematic and highly discordant analyses is highest in the spongy grains and those showing textures classified as “broad altered zoning”, characterized by remnants of broad zoning, often core zoning, which shows alteration at the contact of the different zones (for examples see Fig.

5A).On the other hand, best results were obtained in homogeneous bright portions of the grains (Fig.6).

4.1.2.1. Causes for discordance and dispersion

The zircon dataset shows a remarkable dispersion and even using traditional discordance filters, such as, for example, considering analyses that are no more than 10% discordant, the combined dataset for all samples is spread over an interval of over 1.5 Gyr (3.20 – 1.58 Ga) (Fig. 7A and B). U-Pb dates of granulitic rocks often disclose significant age dispersions and the capability to discriminate between protracted crystallization, age bias due to radiation damage induced Pb-loss and analytical uncertainty is expected. Our data does not describe neither a normal distribution of concordant analyses along the Concordia curve nor a single Discordia trend with well-constrained intercepts (see Fig. 7A). This suggests that multiple populations with different ages were affected by an opening of the isotopic system, resulting in a disposition along the Concordia curve and multiple Discordia trends. A partial resetting of older zircon crystals could have been caused by the amphibolite-facies event recorded in the crystallization of titanite at ca. 2.01 Ga. The crystallization of titanite establishes a geological constraint for the retrometamorphism post-dating the thermal peak of the rocks that have a penetrative metamorphic foliation, that is, the orthogneisses and the amphibolite *boudin* represented by samples TRX-04B, C, and D. This event predates the intrusion of the later pegmatite dyke represented by sample TRX-04A, as evidenced by its lack of a discernible metamorphic foliation and characteristic igneous texture. This is reflected in the combined zircon U-Pb dataset, which can roughly be divided into two distinct groups (Fig. 7A). Results from samples of the metamorphic rocks are characterized by ages predominantly older than 2.1 Ga, with younger ages recorded only in the more discordant analyses. On the other hand, zircons from the pegmatite dyke recorded only a few crystals older than 2.0 Ga, and no results older than 2.3 Ga. These observations confirm the interpretation that the emplacement of the pegmatite dyke took place after the amphibolite-facies re-equilibration recorded by titanite in the orthogneiss and amphibolite. Nonetheless, many zircons of sample TRX-04A show alteration textures and many spot analyses are highly discordant or even needed to be rejected. This implies that at least one event causing widespread partial Pb loss in the U-Pb dataset is not contemporaneous to the crystallization of titanite, and instead post-dates the emplacement of the pegmatite dyke.

The actual age of this event is likely much younger, based on the position close to Neoproterozoic ages of the most discordant crystals along the Concordia curve (Fig. 7A). Because the LAT does not record regional thermal overprint during the Neoproterozoic Brasiliano orogenic cycle, as indicated by Paleoproterozoic K-Ar cooling ages (Siga Jr. 1995), this Pb loss is interpreted to have happened under low-temperature conditions during a hydrothermal event. As zircon is usually very resistant to hydrothermal alteration, the susceptibility of zircon crystals to hydrothermal fluids in low-temperature conditions is strongly controlled by the integrity of the crystalline structure of the mineral (e.g. Rubatto 2017 and references therein). Spontaneous decay of radioactive elements (mainly U and Th) leads to damage of the crystalline structure as alpha-recoil produces small amorphous domains (Nasdala et al. 2001;Palenik et al. 2003). This damage accumulates if the temperature does not allow natural annealing of structure, leading to the progressive metamictization of the crystal. Leaching experiments in metamict zircon show that metamictization produces a significant decrease in stability against hydrothermal fluids (Geisler et al. 2001). Although the zircons analyzed here, including the ones of the pegmatite, have generally low or normal U–contents, the enormous time interval between the magmatic and metamorphic events recorded in the samples (>1.8 Ga) and the assumed hydrothermal event (ca. 600-550 Ma) provides enough time for the accumulation of sufficient radiation damage for the (partial) metamictization of zircon. Hoskin

(2005) estimates that, for U and Th compositions typical of magmatic zircons, time intervals in the order of a few hundreds of Myr would be sufficient to enable hydrothermal Pb disturbance.

Although Pb diffusion can be also very significant in titanite and is affected by radiation damage (Cherniak 1993), this mineral is usually less affected by partial Pb loss and yields therefore often more concordant U-Pb ages than zircon (Tilton and Grünenfelder 1968). This is probably due to differences in annealing and diffusion behavior and typically lower concentrations of U and Th (Howie et al. 1992) and thus lower doses of radiation damage. This may explain the contrast between very concordant titanite and the rather disturbed zircon results observed in our dataset.

Figure 8 displays the relationship between content of radioactive elements (a proxy for the likely intensity of radiation damage, described in terms of effective Uranium: eU = U + 0.235 Th in ppm), U-Pb age, concordance and textures. The figure evidences that different textures predominate in different samples and different age groups. Most young, highly discordant analyses belong to grains with alteration textures (spongy and "broad altered zoning"), particularly in sample TRX-04A. A detailed look on this relation is given by the comparison between the actinide content of each crystal, expressed by its eU which is a proxy for the radiation damage, and the degree of discordance (Fig. 8B) and resulting ages (Fig. 8C, expressed in the more susceptible $^{238}U/^{206}Pb$ system). For the normal discordant U-Pb data (discordance < 100%), mainly belonging to spots with alteration textures, eU correlates strongly with the degree of concordance (Fig. 8B). Similarly, the younger U-Pb ages correlate with eU (Fig. 8C). The correlation is clearer when comparing eU to the degree of concordance than to the overall ages, as the altered grains belong to different age populations. These observations point to the hydrothermal nature of the younger (Neoproterozoic) opening of the U-Pb isotopic system and to radiation damage as main aspect controlling the Pb loss. The correlations are most evident in sample TRX-04A as this sample comprises the highest number of highly discordant analyses and spots on altered textures (see Fig. 8) and furthermore has a more homogeneous age distribution (see below). This sample is therefore the best candidate for an estimate of the timing of the Pb loss by the calculation of a Discordia trend, as will be attempted in Section 4.1.2.2. Note that alteration is also present in the metamorphic samples (TRX-04B/C/D), however less pervasive, so that unaltered spot locations were easier to find, as reflected in their relatively less disturbed dataset.

Because of the probable opening of the U-Pb isotopic system identified in the dataset, additional precautions have to be taken for its interpretation and, particularly, for the calculation of geologically meaningful ages. As discussed by Spencer et al. (2016), the application of traditional discordance filters, such as the acceptance of all analyses ≤10% discordant, for datasets which underwent significant Pb loss can lead to misleading interpretations, especially in ancient samples. One strategy suggested by these authors for dealing with such datasets is to consider only analyses for which the results intersect the Concordia curve within analytical uncertainties. In our dataset, this approach leads to the acceptance of only 35 crystals out of a total of 142 analyses, in a distinct contrast to the population of 92 spot analyses that have ages ≤10% discordant (Fig. 7B). However, comparing the distribution of $^{207}Pb/^{206}Pb$ ages for groups of analyses with different concordance values shows remarkably similar results, even when considering the entire dataset, that is, including strongly discordant analyses (Fig. 7B). The main differences between the different distribution curves are that the main population peaks tend to broaden when including less concordant results, together with a progressive increase in the youngest populations, creating a longer tail that skewers the results towards younger results. Both of these processes are reflective of how small increases in the degree of discordance lead to a higher dispersion of the U-Pb dataset. Nonetheless, the position of the main peaks and their relative prominence remains similar irrespective of the adopted criteria. This shows that the highly concordant analyses, which will be used for refined geological interpretations and age

calculations as they are least affected by Pb loss, are representative of the geochronological signature of the entire dataset in spite of their reduced number. Furthermore, it demonstrates that the adoption of slightly more discordant $^{207}Pb/^{206}Pb$ ages (e.g. up to 10% discordance) is acceptable for subsequent analyses when the consideration of a larger dataset is necessary, such as for the calculation of Hf-based model ages (Section 4.2), as they reproduce the overall distribution of the more precise analyses.

4.1.2.2. Zircon crystallization ages for sample TRX-04A

Only 6 out of 47analysed zircon crystals of sample A have results that intersect the Concordia curve within analytical uncertainty (Fig. 9A).Two spot analyses for rounded /ovoid homogeneous dark crystals give Rhyacian ages (2.29 and 2.16 Ga) that overlap with ages of the high-temperature metamorphic events recorded in the remaining samples (Section 4.1.2.3.) and precede the amphibolite-facies event recorded by the crystallization of titanite. As discussed above, this metamorphic event precedes the emplacement of the pegmatite dyke, and therefore these crystals are considered inherited. The other analyses correspond to two pairs of crystals with Orosirian to Statherian ages at ca. 1.96 Ga and 1.79 Ga that are contemporaneous and younger than the last amphibolite-facies metamorphic event (for exemplary grains and ages see Fig. 5B).

Either of these two sets of ages could represent the actual magmatic age of the dyke, with somewhat different consequences for the geological evolution of the area. If the younger population (1.79 Ga) corresponds to the emplacement, the population at ca. 1.96 would correspond to inherited xenocrysts from a time period that is conspicuously absent from the remaining samples (Fig. 7A and 9A-D). In this sense, if the emplacement of the dyke happened at ca. 1.79 Ga, the crystals at ca. 1.96 Ga could either represent xenocrysts from a restricted magmatism, possibly associated with the amphibolite-facies event at ca. 2.01 Ga, or mixed ages between inherited cores and overgrown rims. Unfortunately, as the grains are either homogeneous dark or spongy, initial textures cannot be detected. On the other hand, if the older population (1.96 Ga) represents the emplacement age, than the younger age should represent magmatic crystals affected by partial Pb loss.

In addition, as discussed in Section 4.1.2.1., sample A is the best candidate to estimate an age for the Neoproterozoic Pb loss. A calculated Discordia trend for sample A (not displayed) has an upper intercept with an age of 2,063 ± 81 Ma and a lower intercept of 515 ± 150 Ma. The remarkably large uncertainties in these intercept ages are probably caused by the fact that there is more than one population of Paleoproterozoic concordant crystals recognized in the sample, preventing the distribution of the data along a single Discordia line. Furthermore, the zircon grains may have suffered some recent Pb loss due to their current exposure to tropical weathering. Nonetheless, the lower value of 515 ± 150 Ma calculated for sample TRX-04A is geologically sensible, as the main geological events that affect the LAT, such as granitic magmatism, shear zone reactivation, development of a volcanic basin, and associated hydrothermalism, all took place during the Brasiliano orogenic cycle between 600 and 560 Ma. The inset in Figure 7C shows how a Neoproterozoic Pb loss event could lead to an age distribution similar to the one observed in sample 04-A.

4.1.2.3. Zircon crystallization ages for samples TRX-04B/C/D

Samples TRX-04B, C and D represent associated lithologies that, in the field and in thin section, are interpreted to have experienced a common geological history during deformation and regional metamorphism. Accordingly, they share complementary U-Pb results, and will be treated together. Out of the 110 spot analyses successfully performed for the three samples, a total of 29 crystals

448 produced results that intercept the Concordia curve within analytical uncertainty (TRX-04B: 12; TRX-
449 04C: 7; TRX-04D: 10). While the different samples record populations that have overlapping ages (Fig.
450 9B-D), each of them has no more than a few analyses in a given sample. Therefore, in order to
451 calculate more precise and statistically robust ages representative of the entire dataset, results from
452 different samples but representative of a same population are considered together.

453 In total, 5 populations are recorded in the three samples, exemplary grains of each population are
454 presented in Figure 5B. The two youngest ones are recorded in the majority of crystals, being
455 identified in all samples. The largest of these is a group of 13 spots with individual ages between 2.21
456 and 2.12 Ga that, together, have a weighted mean age of 2.183 ± 0.017 Ga. The other population
457 consists of 6 crystals with ages from 2.36 to 2.29 Ga, for which a Concordia age was calculated at
458 2.352 ± 0.017 Ga. Because these populations are shared by all samples and represent the youngest
459 concordant crystals recorded in them, they probably represent metamorphic crystallization events,
460 possibly associated with the regional granulite-facies event identified in the LAT.

461 The remaining age populations are more elusive and have a less systematic record in the different
462 samples, ultimately forming a less constrained picture. Ages at ca. 2.5 Ga were recorded only in two
463 crystals in sample TRX-04B, producing a Concordia age of 2.498 ± 0.011 Ga. A somewhat more
464 numerous yet disperse population was identified in five crystals samples TRX-04B and D with
465 individual ages between 2.75 and 2.60 Ga. The best multi-crystal estimate for this population is a
466 rather imprecise weighted mean of 2.683 ± 0.017 Ga. Finally, two inherited cores from sample TRX-
467 04B record stand-alone Meso-to Paleoarchean ages of ca. 3.20 and 3.09 Ga. All of these crystals are
468 interpreted to record the magmatic processes responsible for the generation of the protoliths of the
469 metamorphic samples. The more numerous population probably records the main period of
470 magmatic activity, which already included some degree of recycled crust, as indicated by the
471 presence of two inherited crystals with ages older than 3.0 Ga.

472 Differently from sample TRX-04A, discordant analyses in samples B, C and D are predominantly
473 *reverse* discordant analyses (63 out of 81 discordant analyses), with few *normal* discordant analyses
474 (18 out of 81 discordant analyses). The *normal* discordant analyses fall into the area between the
475 oldest concordant ages, the titanite crystallization and the Neoproterozoic-Cambrian Brasiliano-
476 event (Fig. 7C). The complexity created by the multiple populations and at least one, possibly more
477 Pb-loss events does not allow the calculation of a single Discordia trendline.

478

479 4.1.3.Reverse Discordance

480 Natural reverse discordance is not very common in zircon U-Pb datasets and mainly reported from
481 Archean rocks (Williams et al. 1984; Corfu 2013; Kusiak et al. 2013; Wiemer et al. 2017). In most of
482 the cases reverse discordance seems to be related to high-temperature metamorphism, but Wiemer
483 et al. (2017) present an example where reverse discordance was apparently evoked by a Paleozoic Pb
484 loss event under low T conditions. While the exact mechanism and reasons for reverse discordance
485 remain a matter of debate in the afore mentioned references, it seems that reverse discordance is
486 linked to nano and micro-scale redistribution of radiogenic Pb. Kusiak et al. (2015) observed pure
487 metallic Pb inclusions in zircon which are probably the most extreme case of Pb redistribution.
488 Utsonomiya et al. (2004) report that Pb diffusivity is enhanced when the crystal lattice is already
489 radiation damaged. Wiemer et al. (2017) observe reverse discordance mainly in low eU areas of
490 grains and explain that reverse discordance is produced by migration of radiogenic Pb from high eU
491 areas to low eU areas during a Pb loss -or rather Pb redistribution- event under low T conditions.

In our dataset, reverse discordance occurs mainly in grains / grain areas with homogeneous dark texture (see Fig. 8). There is a clear relationship of reverse discordance with eU with reverse discordance being strongest in very low eU spots (see Fig. 8). This supports the hypothesis that reverse discordance is produced by implantation of radiogenic Pb, as these spots are the most sensitive to the addition of radiogenic Pb, and even the addition of small amounts of radiogenic Pb can have a strong impact on their U/Pb ratios.

Figure 7C indicates how multiple Paleoproterozoic age populations affected by an Neoproterozoic Pb redistribution event could produce a data distribution similar to the one observed in our data set. This supports the idea that in our case, as for Wiemer et al. (2017), reverse discordance was evoked by the same event which caused Pb loss. This event not only caused the damage of the zircon crystalline lattice and the loss of radiogenic material, but caused chemical redistribution inside the crystals, transporting radiogenic Pb from areas rich in U and Th (and thus radiogenic Pb) into areas poor in U, Th and radiogenic Pb, causing reverse discordance in the latter. Preexisting radiation damage of the crystalline structure, accumulated during interval of >1.2 Gyr between zircon crystallization (>1.8 Ga) and the hydrothermal event (600-550 Ma), probably facilitated this process by increasing Pb mobility. Although it seems likely that the Neoproterozoic hydrothermal event was the factor leading to reverse discordance, we cannot exclude that the previous high temperature metamorphism of the rocks played a role, too. More research will be needed in order to better understand the involved processes and their effects.

4.2. Hf isotopic data

Previously dated zircon crystals with the highest degree of concordance of the most frequent age populations were chosen for the measurement and 69 hafnium spot analyses were performed on the same spots as U-Pb analyses. All results can be found in the Electronic Supplement S4.In contrast to the U-Pb analyses, no analytical difficulties were identified complicating the Hf analyses, resulting in overall reliable results. The undisturbed Hf results are in line with observations by Gerdes and Zeh (2009) and Lenting et al. (2010) indicating that Hf isotopes remain nearly unaffected during alteration processes which produce strong Pb loss and disturbed U-Pb ages in zircon.

All but three analyses yield negative $\varepsilon_{Hf}(t1)$ values as low as -16.8, and Hf T_{DM} model ages cover a continuous range from 4.3 to 2.7 Ga (Fig. 11A and B). The detailed description of the results will be performed in the same sample groups as for the U-Pb ages.

4.2.1. Sample A

The 10 Hf spot analyses performed on sample A yield $\varepsilon_{Hf}(t1)$ from -4.2 to -13.6 and T_{DM} model ages from 3.2 - 2.8 Ga (see Fig. 10A). The Hf T_{DM} model ages are rather homogeneous and show no systematic distribution or interdependencies. Reducing the dataset to those analyses in which the U-Pb ellipses intersect the Concordia curve does not change the general distribution of the dataset. The concordant analyses at ca. 1.8 and 2.0 Ga considered to date the emplacement of the pegmatite yield Hf T_{DM} model ages of 3.1-2.8 Ma indicating a long crustal residence.

4.2.2. Samples B/C/D

The $\varepsilon_{Hf}(t1)$ values of samples of metamorphic rocks range from 1.3 to -16.8, with Hf T_{DM} model ages between 4.3 and 2.7 Ga (Fig. 10A). The spot analyses form 2-3 clusters when comparing U-Pb age with $\varepsilon_{Hf}(t1)$. As for sample A, considering only those analyses for which U-Pb ellipses intersect the Concordia does not change the general distribution of the Hf results.

The main cluster is composed of crystals with U-Pb of 2.5-2.0 Ga, ε_{Hf}(t1) values of 1.3 to -11.4 and T_{DM} model ages of 2.7-3.37 Ga. The second cluster is formed by analyses with U-Pb ages > 2.365 and T_{DM} model ages > 3.47 Ga. The oldest inherited cores with U-Pb ages >3 Ga may form a distinct population, but due to the limited amount of data it is not possible to confidently distinguish it from the latter cluster.

Although there is an overall negative correlation of U-Pb ages and ε_{Hf}(t1), the two main clusters share a similar pattern marked by a positive negative correlation between U-Pb age and ε_{Hf}(t1) (see Fig. 10A and B). This suggests two pulses of differentiation and crystallization, each of them starting with the crystallization of more juvenile material followed by an increase in the participation of recycled material. In both clusters, the material with the most crustal signatures (i.e. more recycled material), is added towards the end of each cycle. On the other hand, crystals with the most juvenile signature, characterized by positive ε_{Hf}(t1) values, mark the beginning of the youngest cycle.

The zircon crystallization events at ca. 2.5 Ga and 2.35 Ga (see Fig. 10B) are noteworthy in that they contain Hf signatures from both clusters, indicating that in these events preexisting material was mixed with new and more juvenile material. On the other hand, the event at ca. 2.2 Ga apparently involved a complete mixture of the two endmember compositions: the strongly crustal, recycled material with old model ages (>3.47 Ga) and lag times, as well as the juvenile material with positive ε_{Hf}(t1) which appears the first time at 2.5 Ga.

5. Regional Implications

5.1. Archean and Paleoproterozoic evolution of the LAT

The data presented in this contribution reflect the long and complex evolution of the LAT, as suggested previously by other authors (e.g. Basei et al. 1998a; 2009b; Passarelli et al. 2018). In particular, the wide spread of geologically meaningful crystallization ages even in individual samples illustrates the importance of applying high-resolution geochronological analyses in this type of rock. As such, the new data represents a complement to the available data which, except for a handful of SHRIMP analyses, were predominantly obtained by ID-TIMS (Hartmann 2000; Basei 2009 a, b; Sato et al. 2008). The possibility that some of these analyses performed with traditional methods represent mixed ages is probably responsible for most previous Discordia ages.

Our data confirms that the LAT has a significant ancient signature. Archean ages had been previously obtained with Rb-Sr WR analyses and imprecise upper intercept ages from ID-TIMS Discordias (Siga Jr 1995; Hartmann 1979; Basei 1985; Basei et al. 2009a,b), but high-resolution Archean records were registered in a few SHRIMP U-Pb analyses as old as 2.72 Ga (Hartmann et al. 2000). Our data set includes concordant Mesoarchean ages of 3.0-3.2 Ga and, more significantly, Hf isotopes indicating recycled crustal signatures and differentiation from the mantle in the Hadean or Early Archean. These new Hf T_{DM} model ages are significantly older than existing Sm-Nd T_{DM} model ages, which range from 3.4 to 2.2 Ga (Siga Jr. 1995; Harara 2001; Basei 2009b; Passarelli 2018).

While the oldest ages are restricted to a few zircon xenocrysts, the oldest significant group of ages yields a mean $^{206}Pb/^{207}Pb$ age of 2,683±70 Ma. While Hartmann et al. (2000) argue for two events during the Neoarchean, with magmatism at 2.72 Ga followed by high grade metamorphism at 2.68 Ma, our data does not recognize two distinct populations, instead suggesting a period of prolonged magmatic activity, which agrees with the poly-magmatic evolutions suggested by other authors for different associations of the LAT (e.g. Basei et al. 2009). . Nonetheless, all Archean crystals in our dataset come from samples that experienced an important metamorphic overprint in the Paleoproterozoic and, so far, no undisturbed Archean rocks have been identified in the LAT.

Two concordant analyses seem to record an event for which a Concordia age of 2,498±11 Ma was calculated. Although this age population is small, it stands out for its positive $\varepsilon_{Hf}(t1)$ values (1.3 – 0.6), indicating that this event is significant for the addition of juvenile material. The igneous textures of these grains (oscillatory zoning) and the juvenile Hf signature allow a more precise interpretation and indicate a magmatic origin. Although this age population has only a limited representation in the U-Pb record, the Hf signature of these analyses and of the grains crystallized afterwards (populations of 2.35 and 2.2Ga) suggest that newly differentiated material was added at this time. As mentioned in Section 4.2.1 the zircons of the later events have a Hf signature which seems to be a mixture of the one of the Archean zircons and of the 2.5 Ga population.

The next well-defined zircon population produces a Concordia age of 2,352±23 Ma. Ages around 2350 Ma can be found throughout the Santa Catarina Granulitic Complex and are assigned to a high-grade metamorphic event (Siga Jr 1995; Basei et al. 1998a, 1999, 2000, 2009b). Less than 200 Ma later, around 2180 Ma the Complex was again subject to high grade metamorphism, as suggested previously in the literature (Basei 1985; Siga Jr. 1995; Hartmann et al. 2000; Harara 2001; Sato et al. 2008; Basei et al. 2009a, b).The mean $^{206}Pb/^{207}Pb$ age of 2,183±17 Ma, calculated in this study from 13 spots that intersect the Concordia curve, confirm this interpretation and provide a much more robust age constraint for the event. Individual crystal ages of this population have a rather widespread range (2.21 to 2.12 Ga), preventing the calculation of a Concordia age, and may thus reflect a long-lasting geological event. As the most significant population in our dataset, this event was probably responsible for the present configuration of the LAT as a high-grade metamorphic complex. Together with an abundant Paleoproterozoic record in the region, it may record a long-lived succession of orogenic cycles responsible for the amalgamation of basement associations in southern South America. The Hf T_{DM} model ages of the two latter high-grade metamorphic events range from 2.7 Ga to 3.4 Ga and are, as explained before, probably a mixture of two end-member compositions. They overlap partially with some Sm-Nd T_{DM} model ages presented in the literature (Siga Jr. 1995; Harara 2001; Passarelli 2018)

As mentioned in Section 4.1.1, the titanite mean $^{206}Pb/^{207}Pb$ ages of 1,991±21 Ma and 2,027±28 Ma are interpreted to date the retrograde metamorphism following the high-grade metamorphic peak in the LAT that was responsible for the complete re-equilibration of our samples into an amphibolite-facies paragenesis. Girardi et al. (1974), Basei (1985), Machiavelli et al. (1993), Siga Jr (1995) and Harara (2001) report Pb-Pb and Rb-Sr WR ages of ~2.0 in rocks with little orthopyroxene and conspicuous presence of amphibole as the main mafic mineral, reinforcing this interpretation. Most of these ages have significant analytical errors, and therefore our new titanite U-Pb spot data allows a tighter age constraint of this event between 2.02 and 1.99 Ga.

The emplacement of the pegmatite dyke dated in this study, which took place between 1.96 and 1.79 Ga, goes either along with the end of the retrograde metamorphism or falls in the period of cratonic stabilization described for the LAT. This period is defined by K-Ar cooling ages from hornblende and biotite extracted from multiple expositions of the granulitic complex with ages of 2.1-1.7 Ga and a major concentration around 1.8 Ga for biotite (Girardi et al. 1974; Hartmann et al. 1979; Basei 1985; Machiavelli 1991; Siga Jr 1995; Harara 2001). Concordant Zircon ages of 2.0 or 1.8 Ga are not described in the literature, nor do they appear in the metamorphic samples studied here,indicating that the pegmatite was probably formed by a local magmatic event in the late stages of cratonic stabilization.

5.2. The LAT in the context of the Brasiliano/Pan-African orogenic cycle

The emplacement of the pegmatite dyke constitutes the last significant geological event in the LAT prior to the Neoproterozoic Pan-African/Brasiliano orogenic cycle. The fact that undisturbed

Paleoproterozoic K-Ar ages are recorded even for minerals with low closure temperature such as biotite (*ca.* 310 °C, Harrison et al. 1985) illustrate how the LAT remained remarkably unaffected even during the intense orogenic processes leading to the assembly of Gondwana in the Late Neoproterozoic.

Geological evidences of this event in the LAT affect predominantly its borders. The southern extremity of the terrane is covered by the 650 to 550 Ma old Itajaí Basin (Basei et al. 2010; Guadagnin et al. 2010). The northern portion of the LAT, on the other hand, is patchily intruded by A-type granitoids from the Serra do Mar Suite, which were emplaced at a shallow crustal level between 590 and 570 Ma (Basei et al. 2009; Vlach et al. 2011). In the same region, the Campo Alegre, Corupá and Guaratubinha basins are characterized by a predominance of volcanic and pyroclastic deposits overlying continental sediments. The biggest of these sequences, the Campo Alegre Basin, was deposited between ca. 605 and 585 Ma (Citroni et al. 2001; Quiroz-Valle et al. 2019; Lino et al. in review).

Reflecting this regional pattern, while most of the basement of the LAT records its original subvertical NW-striking structural configuration, both its northern and southern borders have NE-trending structures evidencing a Neoproterozoic overprint (Basei 1985; Harara 2001). In the central portion of the terrane, only localized NE-striking shear zones cross-cut the Santa Catarina Granulitic Complex. These structures are associated with a subordinate population of partially or completely reset K-Ar ages in amphibole and mica, recording an overprint of the geochronological system at ca. 660-620 Ma (Basei et al. 1998, 2009; Passarelli et al. 2018 and references therein). This is mostly attributed to the percolation of hydrothermal fluids along the fault zones, which also controlled the deposition and widespread metasomatic transformations in the Campo Alegre Basin (Lino et al. in review). The same authors propose an age of ca. 565 Ma for the hydrothermal alteration of pyroclastic rocks in this basin, which is in accordance with our interpretation that much of the perturbation of the U-Pb of the present dataset is a possible effect of Neoproterozoic fluid percolation..

The tectonic stability since the Paleoproterozoic, noticeable for a relatively small crustal fragment surrounded by two orogenic belts with extensions of hundreds to thousands of kilometers, has led to the classification of the LAT as a microplate or microcraton during the assembly of West Gondwana (e.g. Basei et al. 1998, 2009, 2010). The lack of a significant Neoproterozoic overprint, in contrast with the highly reworked basement inliers immediately to the north (Curitiba Terrane) was interpreted as an indication that the LAT constitutes an exotic terrane bound by suture zones. The most commonly proposed configuration of this model interprets the LAT and Curitiba Terrane to have been juxtaposed during the Brasiliano Orogenic Cycle along a former subduction zone represented by the Piên Shear Zone (Basei et al. 2000, 2008, 2009, 2018; Passarelli et al. 2018). In this model, the subduction would be responsible for the generation of a magmatic Arc between 615 and 595 Ma (Piên Suite) and the obduction of remnant oceanic crust (Piên mafic-ultramafic Suite) (Harara 2001).

Alternatively, the lack of remnants of passive margin sediments between the LAT and the Curitiba Terrane, together with similarities in the isotopic signatures and Archean to Paleoproterozoic evolution, have been used to propose a common origin for the two terranes, in which their main difference would be the contrasting degrees of tectonic reworking during the Brasiliano Orogenic Cycle (Siga Jr et al. 1993). This model has similarities with recent proposals that suggest a common origin not only for these two terranes, but also for additional basement remnants in southern Brazil and Uruguay, such as the Encantadas and Nico Pérez Terranes (Oyhantçabal et al. 2018; Santos et al. 2019). In this framework, the contrast between basement inliers strongly reworked in the Neoproterozoic, (i.e. Curitiba Terrane, Camboriú Complex, Encantadas Terrane) and more tectonically stable forelands (LAT and Nico Pérez Terranes) has been expressed in terms of varying

metacratonization of the pre-Brasiliano crust (Oriolo et al. 2017; Santos et al. 2019). One paleogeographic reconstruction for the common origin of all these blocks is that they share an affinity with the cratons on the African side of the Pan-African/Brasiliano orogenic systems, particularly the Congo Craton (Oriolo et al. 2016, 2019; Basei et al. 2018; Konopasek et al. 2018; Oyhtançabal et al. 2018). In this model, all of these blocks would share a common geological history in the Paleo- to Mesoproterozoic up to the point, probably in the early Neoproterozoic, in which they were rifted apart. In the model of Basei et al. (2018) this would lead to the generation of oceanic crust and the opening of the Adamastor Ocean. Subsequent closure of this ocean would lead to the collision of the different blocks and a juxtaposition along fault-bound suture zones.

Resuming the discussion above on the comparison between the LAT and the Curitiba Terrane and their combined evolution, the recognition of their common ancient history could provide a synthesis in which both models are not necessarily mutually exclusive. Passarelli et al. (2018) highlight that both terranes differ especially in terms of the contrasting ages for the main migmatization event (Paleoproterozoic vs. Neoproterozoic) and structural configuration (NE-SW striking vs. NW-SE striking). These differences can be interpreted as the result of varying degrees of Neoproterozoic overprint even in a collisional orogenic setting, as long as it involves similar fragments that had previously been rifted apart. In this way, both the evidences indicating subduction and preservation of oceanic crust and the similar ancient origin for both terranes could be accommodated.

6. Conclusion

The new LA-MC-ICP-MS U-Pb data of zircon and titanite presented in this study offer a complement to the existing geochronological database of the basement of the Luis Alves Terrane. Furthermore, we present the first Hf isotope data of this association, which enables a deeper understanding of its evolution.

The critical analysis of the complex U-Pb dataset, supported by Hf analyses, allows a confident interpretation of several magmatic and metamorphic events which formed the LAT. Strongly crustal Hf signatures with ancient model ages are supported by the presence of inherited zircon cores with ages up to 3.2 Ga, giving new constraints on the age of the original extraction of the LAT. Most Archean protoliths were formed at ca. 2.68 Ga, probably during a prolonged magmatic event. Subordinate juvenile accretion took place at ca. 2.5 Ga, supposedly during a second magmatic event, followed by two high-grade metamorphic events at 2.35 and 2.18 Ga responsible for a complete reworking and mixing of the inherited isotopic signatures. A retrograde metamorphic trajectory responsible for the re-equilibration of the metamorphic samples under amphibolite facies conditions is constrained by the crystallization of concordant titanite crystals at 2.02 – 1.99 Ga. Finally, late pegmatitic magmatism is tentatively estimated at between 2.0 and 1.8 Ga.

Zircon grains from all four samples show signs of important hydrothermal alteration. Discordant U-Pb spots suggest that the hydrothermal event happened during the Neoproterozoic Brasiliano orogenic cycle. This hydrothermal event did not only produce Pb loss in the dataset but is probably also responsible for the high number of reverse discordant U-Pb ages observed in the dataset by redistributing radiogenic Pb within the crystals.

Our data reflects how the LAT remained stable during the Pan-African/Brasiliano orogenic cycle in spite of being surrounded by terranes intensively formed or reworked and/or produced in the Late Neoproterozoic, as a disturbance of the U-Pb system was only achieved through a combination of long-term metamictization and hydrothermalism in the samples. Given the proximity of the studied

716 outcrop with the Neoproterozoic Campo Alegre Basin, it is possible that this hydrothermal overprint
717 was a rather local feature.

718

719 **Acknowledgements**

720 This work was funded by FAPESP through the thematic project 2015/03737-0. MH also thanks
721 FAPESP for a current research fellowship (Process 2019/06838-2). BH and MH thank the University of
722 Goettingen, Germany, for logistical and institutional support. The authors thank Fernando Corfu and
723 an unknown reviewer for constructive reviews of the manuscript.

724 **References**

725 Anderson, A.J., Wirth, R., Thomas, R. 2008. The alteration of metamict zircon and its role in the
726 remobilization of high-field-strength elements in the Georgeville granite, Nova Scotia. The
727 Canadian Mineralogist 46(1), 1-18.

728 Almeida, R.P., Janikian, L., Fragoso-Cesar, A.R.S., Fambrini, G.L., 2010. The Ediacaran to Cambrian rift
729 system of Southeastern South America: tectonic implications. The Journal of Geology 118(2),
730 145-161.

731 Basei, M.A.S., 1985. O Cinturão Dom Feliciano em Santa Catarina. PhD Thesis, Universidade de São
732 Paulo.

733 Basei, M.A.S., Siga Jr., O., Reis Neto, J.M. dos, 1990. The Paranagua Batholith: proposition, age,
734 petrogenetic considerations and tectonics implication. In: 36 Congresso Brasileiro de Geologia,
735 Natal. Anais 4, 17 pp.

736 Basei, M.A.S., Siga Jr, O., Machiavelli, A., Mancini, F., 1992. Evolução tectônica dos terrenos entre os
737 Cinturões Ribeira e Dom Feliciano (PR - SC). Revista Brasileira de Geociências 22(2), 216–221.

738 Basei, M.A.S., McReath, I., Siga Jr, O., 1998a. The Santa Catarina granulite complex of southern Brazil:
739 a review. Gondwana Research 1(3-4), 383-391.

740 Basei, M.A.S., Citroni, S.B., Siga Jr, O., 1998b. Stratigraphy and age of Fini-Proterozoic Basins of
741 Paraná and Santa Catarina States, Southern Brazil. Boletim IG-USP. Série Científica 29, 195–
742 216.

743 Basei, M.A.S., Siga Jr, O., Reis Neto, J.M., Passarelli, C.R., Prazeres, H.J., Kaulfuss, G., Sato, K., Lima,
744 O.S., 1999. Paleoproterozoic granulitic belts of the Brazilian southern region (PR-SC). In: II
745 South American Symposium on Isotope Geology—SSAGI, Cordoba, Argentina. Short Papers
746 291–294.

747 Basei, M.A.S., Siga Jr., O., Masquelin, H., Harara, O.M., Reis Neto, J.M., Preciozzi, F., 2000. The Dom
748 Feliciano Belt of Brazil and Uruguay and its Foreland Domain the Rio de la Plata Craton:
749 framework, tectonic evolution and correlation with similar provinces of Southwestern Africa.
750 In: Cordani, U.G., Milani, E.J., Thomaz Filho, A., Campos, D.A. (Eds.), Tectonic Evolution of
751 South America, IGC 31, Rio de Janeiro, 311-334.

752 Basei, M.A.S., Frimmel, H.E., Nutman, A.P., Preciozzi, F., 2008. West Gondwana amalgamation based
753 on detrital zircon ages from Neoproterozoic Ribeira and Dom Feliciano belts of South America
754 and comparison with coeval sequences from SW Africa. In: Pankhurst, R.J., Trouw, R.A.J., de
755 Brito Neves, B.B., de Wit, M.J. (Eds.), West Gondwana: Pre-Cenozoic Correlations Across the
756 South Atlantic Region, London. Geological Society London, Special Publication 294, 239-256.

Basei, M.A.S., Siga Jr, O., Passarelli, C.R., Drukas, C.O., Sato, K., Sproesser, W.M., 2009a. The role of the Curitiba and Luis Alves Microplates during the west Gondwana assembly. In: Simpósio 45 Anos de Geocronologia no Brasil. Boletim de Resumos Expandidos 26–31.

Basei, M.A.S., Nutman, A., Siga Jr, O., Passarelli, C.R., Drukas, C.O., 2009b. The evolution and tectonic setting of the Luis Alves Microplate of Southeastern Brazil: an exotic terrane during the assembly of Western Gondwana. In: Gaucher, C., Sial, A.N., Halverson, G.P., Frimmel, H.E. (Eds.), Neoproterozoic-Cambrian tectonics, global change and evolution: a focus on southwestern Gondwana. Developments in Precambrian Geology 16, 273–291.

Basei, M.A.S., Neves, B.B.B., Junior, O.S., Babinski, M., Pimentel, M.M., Tassinari, C.C.G., Hollanda, M.H.B., Nutman, A., Cordani, U. G., 2010. Contribution of SHRIMP U–Pb zircon geochronology to unravelling the evolution of Brazilian Neoproterozoic fold belts. Precambrian Research 183(1), 112-144.

Basei, M.A.S., Campos Neto, M.C., Castro, N.A., Nutman, A.P., Wemmer, K., Yamamoto, M.T., Hueck, M., Osako, L., Siga, O., Passarelli, C.R., 2011a. Tectonic evolution of the Brusque group, Dom Feliciano belt, Santa Catarina, Southern Brazil. Journal of South American Earth Science 32 (4), 324-350.

Basei, M.A.S., Drukas, C.O., Nutman, A., Wemmer, P.K., Dunyi, L., Santos, P.R., Passarelli, C.R., Campos-Neto, M.C., Siga Jr., O., Osako, L., 2011b. The Itajaí foreland basin: a tectono-sedimentary record of the Ediacaran period, Southern Brazil. International Journal of Earth Sciences 100, 543–569.

Basei, M.A.S., Campos Neto, M.C., Lopes, A.P., Nutman, A.P.,Liu, D., Sato, K. 2013. Polycyclic evolution of Camboriú Complex migmatites, Santa Catarina, Southern Brazil: integrated Hf isotopic and U-Pb age zircon evidence of episodic reworking of a Mesoarchean juvenile crust. Braz. J. Geol., São Paulo 43, 427-443.

Basei, M.A.S.,Frimmel, H., Campos Neto,M.C., Araújo, C.A., Castro,N.A., Passarelli, C.R., 2018. The Tectonic History of the Southern Adamastor Ocean Based on a Correlation of the Kaoko and Dom Feliciano Belts. In: Siegesmund, S., Oyhantçabal, P., Basei, M.A.S., Oriolo, S. (Eds.) Geology of Southwest Gondwana. Regional Geology Reviews, Springer, Heidelberg, 63-85.

Basei, M.A.S, Passarelli, C.R., Hueck M., Siga Jr., O., Fernandes, M.Q. , Araújo de Castro, N., 2020 (in press). Geocronologia e Tectônica do Grupo Brusque – Cinturão Dom Feliciano. In: Bartorelli, A., Teixeira, W., Bley de Brito Neves, B. (Eds.), Geocronologia e Evolução Tectônica do Continente Sul-Americano: a contribuição de Umberto Guiseppe Cordani, Solaris Edições Culturais, São Paulo, 305-333.

Becker-Kerber, B., Paim, P.S.G., Junior, F.C., Girelli, T.J., da Rosa, A.L.Z., El Albani, A., Osés, G.A., Prado, G.M.E.M. ,Figueredo M., Simões, L. S. A., Pacheco, M.L.A.F., 2020. The oldest record of Ediacaran macrofossils in Gondwana (~ 563 Ma, Itajaí Basin, Brazil). Gondwana Research 84, 211-228.

Bitencourt, M.F., Nardi, L.V.S., 2004. The role of xenoliths and flow segregation in the genesis and evolution of the Paleoproterozoic Itapema Granite, a crustally derived magma of shoshonitic affinity from southern Brazil. Lithos 73(1), 1-19.

Campos Neto, M.D.C., Figueiredo, M.D., 1995. The Rio Doce Orogeny, Southeastern Brazil. Journal of South American Earth Sciences 8(2), 143-162.

Campos Neto, M.C., 2000, Orogenic systems from Southwestern Gondwana, an approach to Brasiliano-Pan African cycle and orogenic collage in Southeastern Brazil. In: Cordani, U.G., Milani, E.J., Thomaz Filho, A., Campos, D.A. (Eds.), Tectonic Evolution of South America, IGC 31, Rio de Janeiro, 335-365.

Cherniak, D.J., 1993. Lead diffusion in titanite and preliminary results on the effects of radiation damage on Pb transport. Chemical Geology 110(1-3), 177-194.

Citroni, S.B., Basei, M.A.S., Siga Jr, O., Reis Neto, J.M., 2001. Volcanism and stratigraphy of the Neoproterozoic Campo Alegre basin, SC, Brazil. Anais da Academia Brasileira de Ciências 73(4), 581-597.

Corfu, F., 2013. A century of U-Pb geochronology: The long quest towards concordance. GSA Bulletin 125(1-2), 33-47.

Corfu, F., Hanchar, J.M., Hoskin, P.W., Kinny, P., 2003. Atlas of zircon textures. Reviews in mineralogy and geochemistry 53(1), 469-500.

Costa, M.S., Nascimento, M.S., 2015. Tratos deposicionais e arquitetura estratigráfica de sucessões sedimentares da Bacia do Itajaí (Neoproterozoico), nordeste de Santa Catarina, Brasil. Geologia USP, série científica 15(2), 111-134.

Cury, L.F., Siga, O., Harara, O.M., Sato, K., Basei, M.A.S., 2008. Geological and geochronological setting of Paranaguá Domain, Ribeira Belt – Southern Brazil. 33 International Geological Congress, Oslo, CD–ROM.

Florisbal, L.M., Janasi, V.A., Bitencourt, M.F., Nardi, L.V.S., Heaman, L.M., 2012a. Contrasted crustal sources as defined by whole-rock and Sr–Nd–Pb isotope geochemistry of Neoproterozoic early post-collisional granitic magmatism within the Southern Brazilian Shear Belt, Camboriú, Brazil. Journal of South American Earth Science 39, 24-43.

Florisbal, L.M., Janasi, V.A., Bitencourt, M.F., Heaman, L.M., 2012b. Space-time relation of post-collisional granitic magmatism in Santa Catarina, southern Brazil: U-Pb LAMC-ICP-MS zircon geochronology of coeval mafic-felsic magmatism related to the Major Gercino Shear Zone. Precambrian Research 216-219, 132-151.

Fornari, A., 1998. Geologia e metalogenese da porção meridional do craton Luis Alves-SC. PhD thesis, State University of Campinas, Brazil.

Frost, B.R., Chamberlain, K.R., Schumacher, J.C., 2001. Sphene (titanite): phase relations and role as a geochronometer. Chemical geology 172 (1-2), 131-148.

Girardi, V.A.V., Cordani, U.G., Candido, A., Melfi, A.J., Kawashita, K., 1974. Geocronologia do Complexo Basico-Ultrabasico pré-brasiliano de Pien, PR. In: 29° Congresso Brasileiro de Geologia. Porto Alegre. Resumos 532-533.

Girardi, V.A.V., Ulbrich, H.H.G.J., 1978. A saphirine-orthopyroxene spinel occurrence in the Pien Area, Paraná, southern Brazil. Revista Brasileira de Geociências 8, 284–293.

Guadagnin F., Chemale Jr. F., Dussin I.A., Jelinek A.R., Santos M.N., Borba, M.L., Justino D., Bertotti A.L., Alessandretti L., 2010. Depositional age and provenance of the Itajaí Basin, Santa Catarina State, Brazil: Implications for SW Gondwana correlation. Precambrian Research 180, 156-182.

838 Gualda, G.A., Vlach, S.R., 2007a. The Serra da Graciosa A-type Granites and Syenites, southern Brazil.
839 Part 1: Regional setting and geological characterization. Anais da Academia Brasileira de
840 Ciências 79(3), 405-430.

841 Gualda, G.A., Vlach, S.R., 2007b. The Serra da Graciosa A-type Granites and Syenites, southern Brazil:
842 Part 2: Petrographic and mineralogical evolution of the alkaline and aluminous
843 associations. Lithos 93(3-4), 310-327.

844 Geisler, T., Ulonska, M., Schleicher, H., Pidgeon, R.T., van Bronswijk, W., 2001. Leaching and
845 differential recrystallization of metamict zircon under experimental hydrothermal conditions.
846 Contributions to Mineralogy and Petrology 141(1), 53-65.

847 Geisler, T., Rashwan, A.A., Rahn, M.K.W., Poller, U., Zwingmann, H., Pidgeon, R.T., Schleicher, H.,
848 Tomaschek, F., 2003. Low-temperature hydrothermal alteration of natural metamict zircons
849 from the Eastern Desert, Egypt. Mineralogical Magazine 67(3), 485-508.

850 Gerdes, A., Zeh, A., 2009. Zircon formation versus zircon alteration—new insights from combined U–
851 Pb and Lu–Hf in-situ LA-ICP-MS analyses, and consequences for the interpretation of Archean
852 zircon from the Central Zone of the Limpopo Belt. Chemical Geology, 261(3-4), 230-243.

853 Hallinan, S.E., Mantovani, M.S., Shukowsky, W., Braggion Jr, I., 1993. Estrutura do Escudo Sul-
854 Brasileiro: uma revisão através de dados gravimétricos e magnetométricos. Revista Brasileira
855 de Geociências, 23(3), 201-214.

856 Harara, O.M., 1996. Análise estrutural, petrológica e geocronológica dos litotipos da região de Piên
857 (PR) e adjacências. Unpub. Masters dissertation, Univcrsidade de São Paulo. 196 p.

858 Harara, O.M.M., 2001. Mapeamento e investigação petrológica e geocronológica dos litotipos da
859 região do Alto Rio Negro (PR-SC): um exemplo de sucessivas e distintas atividades magmáticas
860 durante o Neoproterozóico. PhD thesis, Universidade de São Paulo.

861 Harara, O.M.M., Basei, M.A.S., Siga Jr, O., Campos Neto, M.d.C., Prazeres Filho, H.J.d, 2003. Dating of
862 high grade metamorphism by U-Pb, Sm-Nd and K-Ar isotopic systems: Paleoproterozoic I-type
863 granulites from the northern border of the Luis Alves Gneiss-Granulite Terrane, Southern
864 Brazil. In: IV South American Symposium on Isotope Geology, Salvador, Short Papers II, 568-
865 571.

866 Harrison, T.M., Duncan, I., McDougall, I., 1985. Diffusion of 40Ar in biotite: Temperature, pressure
867 and compositional effects. Geochimica et Cosmochimica Acta 49, 2461-2468.

868 Hartmann, L.A., Silva, L.C., Orlandi Filho, V., 1979. O Complexo Granultico de Santa Catarina.
869 Descricao e implicacoes genteticas. Acta Geol. Leopoldensia 3, 93–112.

870 Hartmann, L., Basei, M.,Simas, M., 1998. Geochemistry of the Lower Protezoroic Granulite-Facies
871 Grant Syenite Gneiss, Barra Velha, Santa Catarina State, Southern Brazil. Pesquisas em
872 Geociências 25(2), 3-9.

873 Hartmann, L.A., Santos, J.O., McNaughton, N.J., Vasconcellos, M.A., Silva, L.C., 2000. Ion microprobe
874 (SHRIMP) dates complex granulite from Santa Catarina, southern Brazil. Anais da Academia
875 Brasileira de Ciências 72(4), 559-572.

876 Heilbron, M., Pedrosa-Soares, A.C., Campos Neto, M.D.C., Silva, L.D., Trouw, R.A.J., Janasi, V.D.A.,
877 2004. Província Mantiqueira. In: Geologia do continente sul-americano: evolução da obra de
878 Fernando Flávio Marques de Almeida, 203-235.

879 Hoskin, P.W., 2005. Trace-element composition of hydrothermal zircon and the alteration of Hadean
880 zircon from the Jack Hills, Australia. Geochimica et Cosmochimica Acta 69(3), 637-648.

881 Hoskin, P.W.O., Black, L.P., 2000. Metamorphic zircon formation by solid-state recrystallization of
882 protolith igneous zircon. Journal of metamorphic Geology 18(4), 423-439.

883 Howie, R.A., Zussman, J., Deer, W., 1992. An introduction to the rock-forming minerals, Longman, p.
884 696

885 Hueck, M., Basei, M.A.S., de Castro, N.A., 2016. Origin and evolution of the granitic intrusions in the
886 Brusque Group of the Dom Feliciano Belt, south Brazil: Petrostructural analysis and whole-
887 rock/isotope geochemistry. Journal of South American Earth Sciences 69, 131-151.

888 Hueck, M., Oyhantçabal, P., Philipp, R.P., Basei, M.A.S., Siegesmund, S., 2018. The Dom Feliciano Belt
889 in Southern Brazil and Uruguay. In: Siegesmund, S., Oyhantçabal, P., Basei, M.A.S., Oriolo, S.
890 (Eds.) Geology of Southwest Gondwana. Regional Geology Reviews, Springer, Heidelberg, 267-
891 302.

892 Hueck, M., Basei, M.A.S., Castro, N.A., 2020. Tracking the sources and the evolution of the late
893 Neoproterozoic granitic intrusions in the Brusque Group, Dom Feliciano Belt, South Brazil: LA-
894 ICP-MS and SHRIMP geochronology coupled to Hf isotopic analysis. Precambrian Research 338.

895 Kaul, P.F.T., 1984. Significado dos granitos anorogênicos da Suíte Intrusiva Serra do Mar na evolução
896 da crosta do sul-sudeste do Brasil, no âmbito das folhas SG-22, Curitiba e SG-23, Iguape. In: 33
897 Congresso Brasileiro de Geologia, Rio de Janeiro. Resumos 2815–2825.

898 Kaul, P.F.T., 1997. O magmatismo na Serra do mar e Adjacências (Sul do Brasil) no final do
899 Proterozoico e seus condicionantes tectônicos. PhD thesis, Universidade de São Paulo.

900 Kohn, M.J., 2017. Titanite petrochronology. Reviews in Mineralogy and Geochemistry 83(1), 419-441.

901 Konopásek, J., Janoušek, V., Oyhantçabal, P., Sláma, J., Ulrich, S., 2018. Did the circumrodinia
902 subduction trigger the Neoproterozoic rifting along the Congo–Kalahari Craton
903 margin?. International Journal of Earth Sciences 107(5), 1859-1894.

904 Kröner, A., Wan, Y., Liu, X., Liu, D., 2014. Dating of zircon from high-grade rocks: Which is the most
905 reliable method? Geoscience Frontiers 5(4), 515-523.

906 Kusiak, M.A., Whitehouse, M.J., Wilde, S.A., Nemchin, A.A., Clark, C., 2013. Mobilization of radiogenic
907 Pb in zircon revealed by ion imaging: Implications for early Earth geochronology. Geology
908 41(3), 291-294

909 Kusiak, M.A., Dunkley, D.J., Wirth, R., Whitehouse, M.J., Wilde, S.A., Marquardt, K., 2015. Metallic
910 lead nanospheres discovered in ancient zircons. Proceedings of the National Academy of
911 Sciences, 112(16), 4958-4963.

912 Laurent, A., Bingen, B., Duchene, S., Whitehouse. M.J., Seydoux-Guillaume, A.-M., Bosse, V. 2018.
913 Decoding a protracted zircon geochronological record in ultrahigh temperature granulite, and
914 persistence of partial melting in the crust, Rogaland, Norway. Contrib. Mineral. Petrol. 173, 29.

915 Lenting, C., Geisler, T., Gerdes, A., Kooijman, E., Scherer, E.E., Zeh, A., 2010. The behavior of the Hf
916 isotope system in radiation-damaged zircon during experimental hydrothermal alteration.
917 American Mineralogist, 95(8-9), 1343-1348.

918 Lino, L.M., Quiroz-Vale, F.R., Louro, V., Basei, M.A.S., Vlach, S.R.F., Hueck, M., Muñoz, P.R.M., Citroni,
919 S.B. Structural architecture and the episodic evolution of the Ediacaran Campo Alegre Basin
920 (southern Brazil): Implications for the development of a synorogenic foreland rift and a post-
921 collisional caldera volcano. In review at the Journal of South American Earth Science on July
922 15th 2020.

923 Ludwig, K.R., 2001. Using Isoplot/Ex. A Geochronological Toolkit for Microsoft Excel. Berkeley
924 Geochronology Center, Special Publications No. 1, Berkeley, USA.

925 Machiavelli, A., 1991. Os Granitóides Deformados da Região de Pien (PR): Um provável Arco
926 Magmático do Proterozóico Superior. MSc Dissertation, University of São Paulo, 89 pp.

927 Machiavelli, A., Basei, M.A.S., Siga Jr. O., 1993. Suite Granitica Rio Pien: um arco magmático do
928 Proterozóico Superior na Microplaca Curitiba. Geochim. Brasiliensis 7 (2), 113–129.

929 Martini, A., Bitencourt, M.F., Nardi, L.V.S., Florisbal, L.M., 2015. An integrated approach to the late
930 stages of Neoproterozoicpost-collisional magmatism from Southern Brazil: Structural
931 geology,geochemistry and geochronology of the Corre-mar Granite. Precambrian Research
932 261, 25-39.

933 Martini, A., de Fátima Bitencourt, M., Weinberg, R.F., De Toni, G.B., Lauro, V.N., 2019. From
934 migmatite to magma-crustal melting and generation of granite in the Camboriú Complex,
935 south Brazil. Lithos 340, 270-286.

936 Minioli, B., 1972. Aspectos Geológicos da regiao litoranea de Piçarras, Barra Velha, SC. PhD Thesis,
937 University of São Paulo, 104 pp.

938 Nasdala, L., Wenzel, M., Vavra, G., Irmer, G., Wenzel, T., Kober, B., 2001. Metamictisation of natural
939 zircon: accumulation versus thermal annealing of radioactivity-induced damage. Contributions
940 to Mineral Petrology 141, 125-144.

941 Nasdala, L., Hanchar, J.M., Rhede, D., Kennedy, A.K., Váczi, T., 2010. Retention of uranium in
942 complexly altered zircon: An example from Bancroft, Ontario. Chemical Geology 269 (3-4),
943 290–300.

944 Oriolo, S., Oyhantçabal, P., Basei, M.A.S., Wemmer, K., Siegesmund, S., 2016. The Nico Pérez Terrane
945 (Uruguay): From Archean crustal growth and connections with the Congo Craton to late
946 Neoproterozoic accretion to the Río de la Plata Craton. Precambrian Research 280, 147-160.

947 Oriolo, S., Oyhantçabal, P., Wemmer, K., Siegesmund, S., 2017. Contemporaneous assembly of
948 Western Gondwana and final Rodinia break-up: Implications for the supercontinent
949 cycle. Geoscience Frontiers 8(6), 1431-1445.

950 Oriolo, S., Oyhantçabal, P., Konopásek, J., Basei, M.A., Frei, R., Sláma, J., Wemmer, K., Siegesmund, S.,
951 2019. Late Paleoproterozoic and Mesoproterozoic magmatism of the Nico Pérez Terrane
952 (Uruguay): Tightening up correlations in southwestern Gondwana. Precambrian Research 327,
953 296-313.

Oyhantçabal, P., Siegesmund, S., Wemmer, K., Presnyakov, S., Layer, P., 2009. Geochronological constraints on the evolution of the southern Dom Feliciano Belt (Uruguay). Journal of the Geological Society of London 166, 1075–1084.

Oyhantçabal, P., Oriolo, S., Philipp, R.P., Wemmer, K., Siegesmund, S., 2018. The Nico Pérez Terrane of Uruguay and Southeastern Brazil. In: Siegesmund, S., Oyhantçabal, P., Basei, M.A.S., Oriolo, S. (Eds.) Geology of Southwest Gondwana. Regional Geology Reviews, Springer, Heidelberg, 161-188.

Palenik, C.S., Nasdala, L., Ewing, R.C., 2003. Radiation damage in zircon. American Mineralogist 88 (5-6), 770-781.

Passarelli, C.R., Basei, M.A.S., Neto, M.D.C.C., Júnior, O.S., Prazeres Filho, H.J., 2004. Geocronologia e geologia isotópica dos terrenos Pré-Cambrianos da porção sul-oriental do Estado de São Paulo. Geologia USP. Série Científica 4(1), 55-74.

Passarelli, C.R., Basei, M.A.S., Wemmer, K., Siga Jr., O., Oyhantçabal, P., 2011. Major Shear Zones of southern Brazil and Uruguay: escape tectonics in the eastern border of Rio de La Plata and Paranapanema cratons during the Western Gondwana amalgamation. International Journal of Earth Sciences (Geol.Rundsch) 100, 391-414.

Passarelli, C.R, Basei, M.A.S., Siga Jr., O., Harara, M.M., 2018. The Luis Alves and Curitiba Terranes: Continental Fragments in the Adamastor Ocean. In: Siegesmund, S., Oyhantçabal, P., Basei, M.A.S., Oriolo, S. (Eds.) Geology of Southwest Gondwana. Regional Geology Reviews, Springer, Heidelberg, 161-188.

Philipp, R.P., Mallmann, G., Bitencourt, M.F., Souza, E.R., Souza, M.M.A., Liz, J.D., Wild, F., Arendt, S., Oliveira, A., Duarte, L., Rivera, C.B., Prado, M., 2004. Caracterização litológica e evolução metamórfica da porção leste do Complexo Metamórfico Brusque, Santa Catarina. Revista Brasileira de Geociências 34, 21-34.

Philipp, R.P., Pimentel, M.M., Chemale Jr., F., 2016. Tectonic evolution of the Dom Feliciano Belt in Southern Brazil: Geological relationships and U-Pb geochronology. Brazilian Journal of Geology 46 (1), 83-104.

Quiroz-Valle, F.R., Basei, M.A.S., Lino, L.M., 2019. Petrography and detrital zircon U-Pb geochronology of sedimentary rocks of the Campo Alegre Basin, Southern Brazil: implications for Gondwana assembly. Brazilian Journal of Geology 49(1).

Rostirolla, S.P., Ahrendt, A., Soares, P.C., Carmingnani, L., 1999. Basin analysis and mineral endowment of the Proterozoic Itajaí Basin, south-east Brazil. Basin Research 11, 127–142.

Rubatto, D., 2017. Zircon: the metamorphic mineral. In: Kohn, M.J., Engi, M., Lanari, P. (Eds.) Petrochronology. Reviews in mineralogy and geochemistry 83(1), 261-295.

Santos, J.O., Chernicoff, C.J., Zappettini, E.O., McNaughton, N.J., Hartmann, L.A., 2019. Large geographic and temporal extensions of the Río de la Plata Craton, South America, and its metacratonic eastern margin. International Geology Review 61(1), 56-85.

Sato, K., Williams, I., Hyder, J., Yaxley, G., Cordani, U.G., Tassinari, C.C.G., Basei, M.A.S., Siga Jr, O., 2008. Multicollector SHRIMP IIe of Brazil—first results. In: VI South American Symposium on Isotope Geology – SSAGI 2008, Bariloche. Abstracts.

Siegesmund, S., Oyhantçabal, P., Basei, M.A.S., Oriolo, S., 2018. Geology of Southwest Gondwana. Regional Geology Reviews, Springer, Heidelberg.

Siga Jr., O., 1995. Dominios Tectónicos do Sudeste do Paraná e Nordeste de Santa Catarina: Geocronologia e Evolucao Crustal. PhD Thesis, Universidade de São Paulo, 212 pp.

Siga Jr, O., Basei, M.A., Machiavelli, A., 1993. Evolução geotectônica da porção NE de Santa Catarina e SE do Paraná, com base em interpretações geocronológicas. Revista Brasileira de Geociências 23(3), 215-223.

Siga Jr, O., Basei, M.A.S., Reis Neto, J.M., Harara, O.M., Passarelli, C.R., Prazeres Filho, H. J., Weber, W., Machiavelli, A., 1997. Ages and tectonic setting of alkaline—peralkaline granitoids of Paraná and Santa Catarina states, southern Brazil. In South American Symposium on Isotope Geology, Campos do Jordão, Brazil, Short Papers, 301-303.

Siga Jr, O., Basei, M.A.S., Sato, K., Citroni, S.B., Reis Neto, J.M., Weber, W., Lima, P.S., Sproesser, W.M., 1999. Post-orogenic magmatism and sedimentation in Neoproterozoic extensional regimes in the Brazilian southern region. In: II South American Symposium on Isotope Geology – SSAGI 1999, Cordoba. Abstracts, 367–370.

Silva, L.C. da, 1984. Os terrenos de médio e alto grau do Pré-Cambriano de Santa Catarina. In: 33 Congresso Brasileiro de Geologia, Rio de Janeiro. Anais 3, 3069-3080.

Silva, L.C. da, Hartmann, L.A., McNaughton, N.J., Fletcher, I., 2000. Zircon U-Pb SHRIMP dating of a Neoproterozoic overprint in Paleoproterozoic granitic-gneissic terranes, southern Brazil. American Mineralogist 85, 649-667.

Spencer, C.J., Kirkland, C.L., Taylor, R.J., 2016. Strategies towards statistically robust interpretations of in situ U–Pb zircon geochronology. Geoscience Frontiers 7(4), 581-589.

Taylor R.J.M., Kirkland C.L., Clark C., 2016. Accessories after the facts: Constraining the timing, duration and conditions of high-temperature metamorphic processes. Lithos 264, 239–257.

Tedeschi M., Pedrosa-Soares A., Dussin I., Lanari P., Novo T., Pinheiro M. A. P., Lana C., Peters D., 2018. Protracted zircon geochronological record of UHT garnet-free granulites in the Southern Brasília orogen (SE Brazil): Petrochronological constraints on magmatism and metamorphism. Precambrian Research 316, 103–126.

Tilton, G.R., and Grünenfelder, M.H., 1968. Sphene: Uranium-lead ages. Science 159(3822), 1458-1461.

Utsunomiya, S., Palenik, C.S., Valley, J.W., Cavosie, A.J., Wilde, S.A., Ewing, R.C., 2004. Nanoscale occurrence of Pb in an Archean zircon. Geochimica et Cosmochimica Acta 68(22), 4679-4686.

Vlach, S.R., Siga Jr, O., Harara, O.M., Gualda, G.A., Basei, M.A., Vilalva, F.C., 2011. Crystallization ages of the A-type magmatism of the Graciosa Province (Southern Brazil): Constraints from zircon U-Pb (ID-TIMS) dating of coeval K-rich gabbro-dioritic rocks. Journal of South American Earth Sciences 32(4), 407-415.

Whitehouse M., Kemp A.I.S., 2010. On the difficulty of assigning crustal residence, magmatic protolith and metamorphic ages to Lewisian granulites: constraints from combined in situ U-Pb and Lu–Hf isotopes. Geol. Soc., London, Spec. Publ. 335, 81–101.

Wiemer, D., Allen, C.M., Murphy, D.T., Kinaev, I., 2017. Effects of thermal annealing and chemical abrasion on ca. 3.5 Ga metamict zircon and evidence for natural reverse discordance: Insights for U-Pb LA-ICP-MS dating. Chemical Geology 466, 285-302.

Williams, I.S., Compston, W., Black, L.P., Ireland, T.R., Foster, J.J., 1984. Unsupported radiogenic Pb in zircon: a cause of anomalously high Pb-Pb, U-Pb and Th-Pb ages. Contributions to Mineralogy and Petrology 88(4), 322-327.

Zhao, L., Li, T., Peng, P., Guo, J., Wang, W., Wang, H., Santosh, M., Zhai, M., 2015. Anatomy of zircon growth in high pressure granulites: SIMS U–Pb geochronology and Lu–Hf isotopes from the Jiaobei Terrane, eastern North China Craton. Gondwana Research, 28(4), 1373-1390.

Figures and Captions

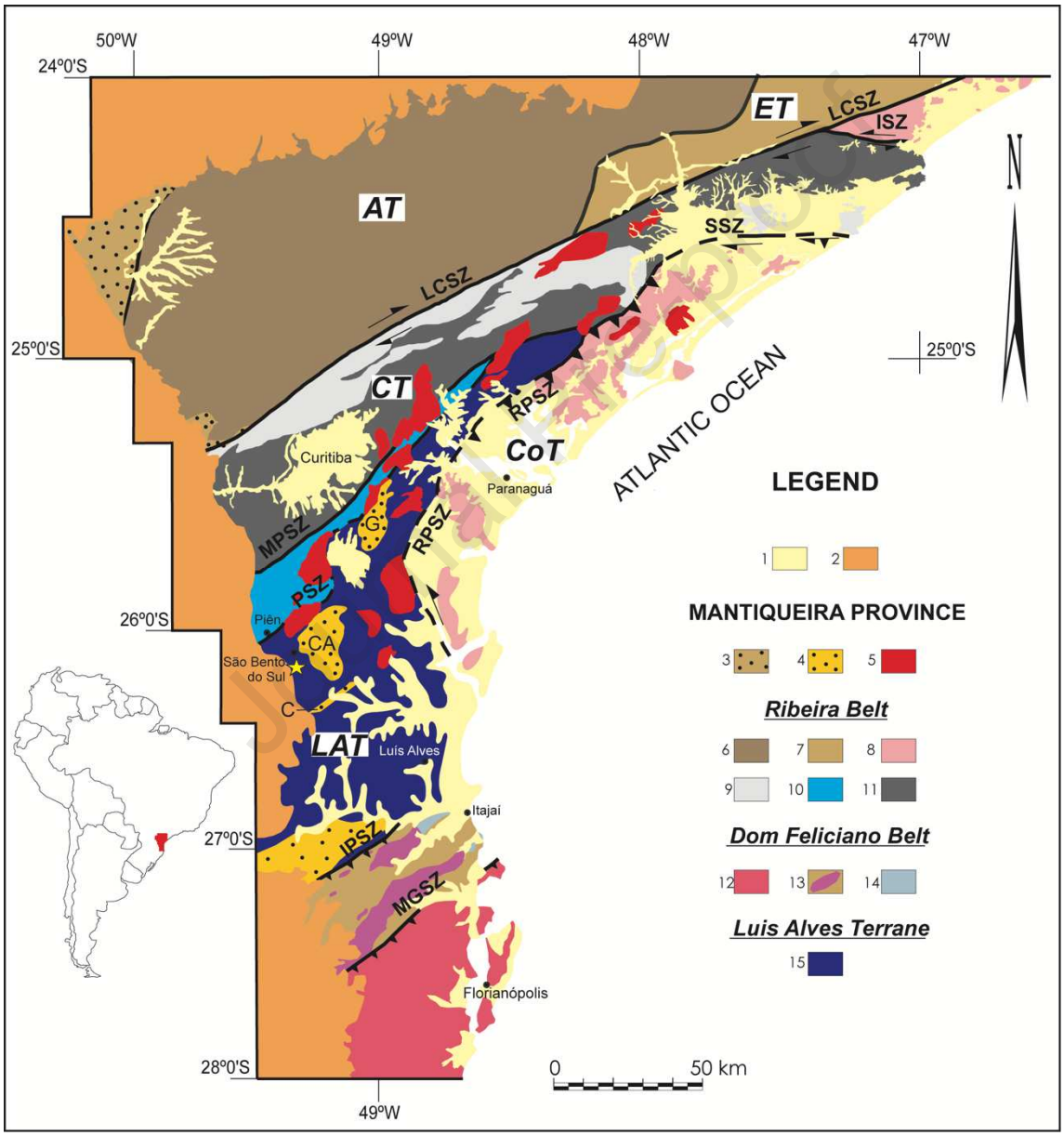

Fig. 1 –Tectonic and geological sketch of the south-southeast Brazilian Precambrian terranes with sampling location of sample TRX-04 (star). 1. Quaternary and Tertiary sediments; 2. Paraná Basin; 3. Eopaleozoic basins; 4. Neoproterozoic basins (CA: Campo Alegre; C: Corupá; G: Guaratubinha); 5. Graciosa/Serra do Mar Suite alkaline granites. ***Ribeira Belt*****: Apiaí Terrane (AT)**: 6. Supracrustal and granitic rocks undifferentiated. **Embu Terrane (ET)**: 7. Orthogneisses, supracrustal and granitic rocks undifferentiated. **Coastal Terrane (CoT)**: 8. Metassedimentary Sequences and gneiss-granitic rocks of Paranaguá/Mongaguá Domains undifferentiated. **Curitiba Terrane (CT)**: 9. Supracrustal rocks; 10. Piên Domain: calc-alkaline granitoids and mafic ultramafic suite; 11. Atuba-Registro Itatins Complexes. ***Dom Feliciano Belt***: 12. Granitoid belt (Florianópolis Batholith); 13.

Schist Belt and intrusive granitoids; 14. Basement inliers. ***Luís Alves Terrane (LAT)***: 15. Santa Catarina granulitic Complex. **Main shear zones (SZ)**: LCSZ: Lancinha-Cubatão; ISZ: Itariri; SSZ: Serrinha; RPSZ: Rio Palmital; MPSZ: Mandirituba-Piraquara; PSZ: Piên; IPSZ: Itajaí-Perimbó; MGSZ: Major Gercino. Modified from Passarelli et al. (2018). Based on Basei (2000); Basei et al. (1992), (2000), (2009b); Campos Neto and Figueiredo (1995).

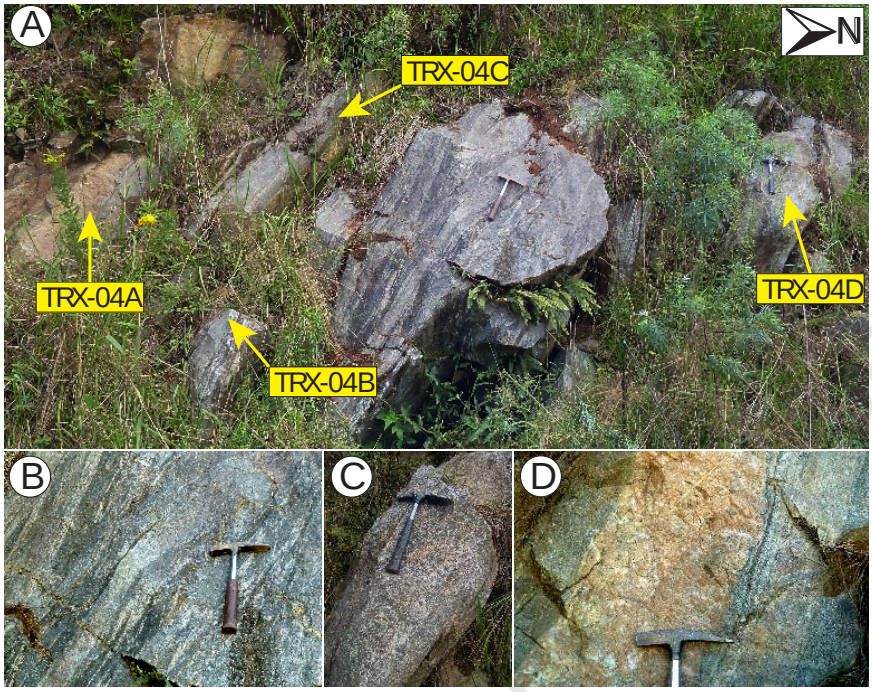

Fig. 2 – Field pictures of the sampled rocks. (A) Entire outcrop representative of the metamorphic units; the yellow arrows indicate the location of the collected samples. (B) orthogneiss in the center of the outcrop. Samples TRX-04B and TRX-04B are homogeneous, slightly broader felsic (TRX-04B) and mafic (TRX-04C) bands of this gneiss. (C) amphibolite lens, sample TRX-04D. (D) detail picture of the pegmatite, sample TRX-04A.

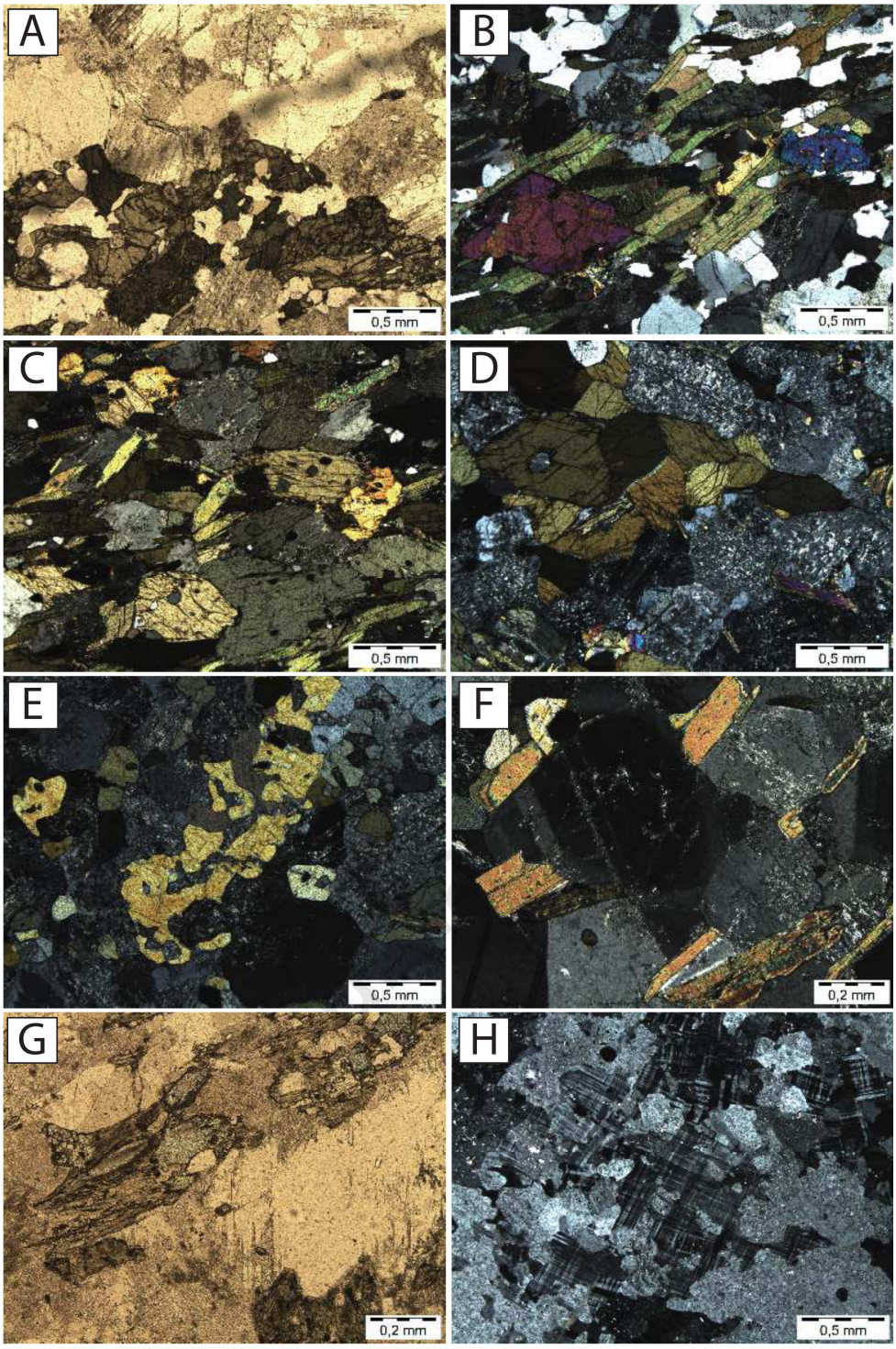

Fig. 3 – Microphotographs of TRX-04 outcrop samples. **Sample TRX-04B**: (a) Anhedral amphiboles in quartz–feldspatic groundmass of the syenogranite-gneiss TRX-04B. The feldspars look darker because they are very altered. (b): Euhedral epidote with zoning (pink), aligned biotite, feldspar and quartz. **Sample TRX-04C** (c): Orientated, inclusion rich amphiboles with some biotite and altered feldspar in the quartz-monzonitic gneiss. **Sample TRX-04D (amphibolite)**: (d) aggregation of several amphiboles in the middle of very saussuritized plagioclases, (e) Epidote associated to calcite with altered, sometimes tabular plagioclase, (f) The dark plagioclase in the middle shows a hexagonal zoning. Note the 120° angles where 3 grains meet (g) Intergrowth of epidote and biotite. **Sample TRX-04A** (h) Microcline and strongly altered orthoclase (or plagioclase, a clear discrimination is often not possible) in the pegmatite sample TRX-04 A.

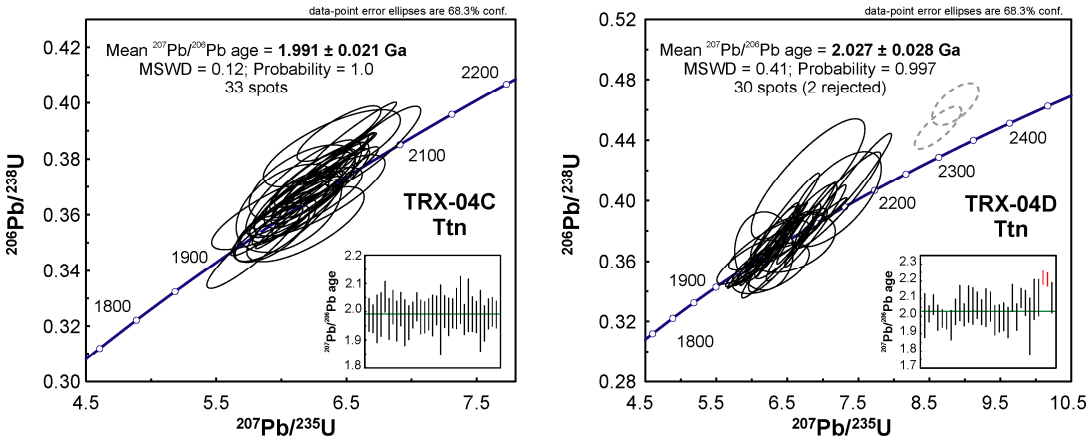

Figure 4: Concordia diagrams and mean age plots of the titanite U-Pb dataset. Spots used for age calculations are represented as empty black ellipses and empty dashed grey ellipses and red lines in the mean age plot represent discarded analyses.

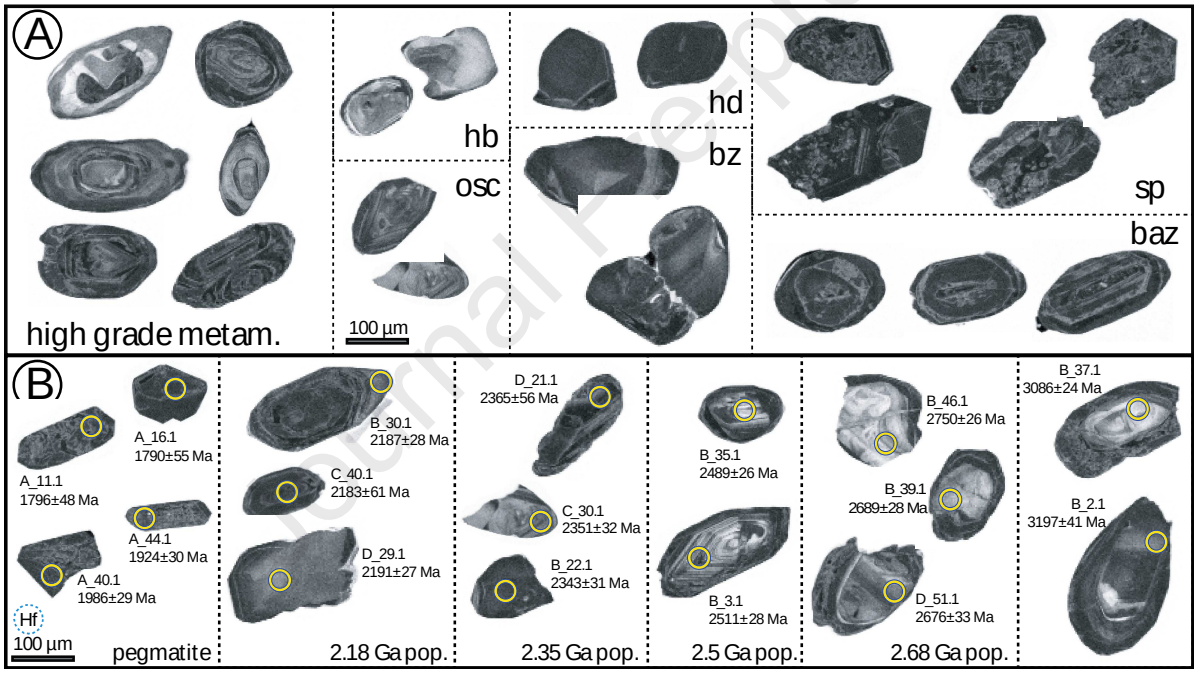

Figure 5: CL images of zircon grains from all samples, scaling is the same in A and B. (A) shows examples of the variety of different textures present the samples. The grains in the left panel show very complex, often chaotic textures typical for high grade metamorphism and cores overprinted by zones of recrystallization or new growth, the others show examples of each classification (hb: homogeneous bright, hd: homogeneous dark, osc: oscillatory zoning, bz: broad zoning, sp: spongy/porous, baz: broad altered zoning). (B) shows highly concordant (intercept with Concordia) grains and ages of each age population. The circles show the 32 µm sized LA spots for the U-Pb analyses. Hf analyses were performed with 47 µm sized LA spots (dashed circle next to scale bar) in the same locations. The corresponding analytical data can be found in the electronic supplementary material.

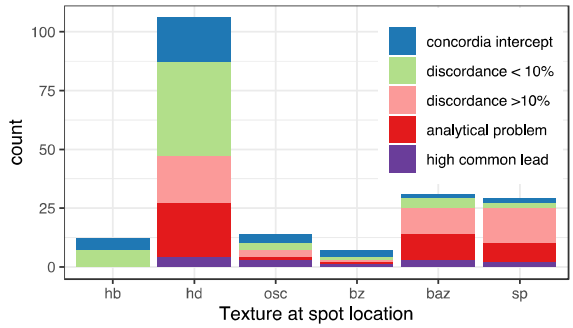

Figure 6: Barplot showing the distribution of textures of all samples indicating the proportion of concordant, discordant and problematic analyses (baz: broad altered zoning, bz: broad zoning, hb: homogeneous bright, hd: homogeneous dark, osc: oscillatory zoning, sp: spongy/porous). Highly discordant (>10%) and problematic analyses are mainly related to grains with alteration features such as spongy texture or broad altered zoning.

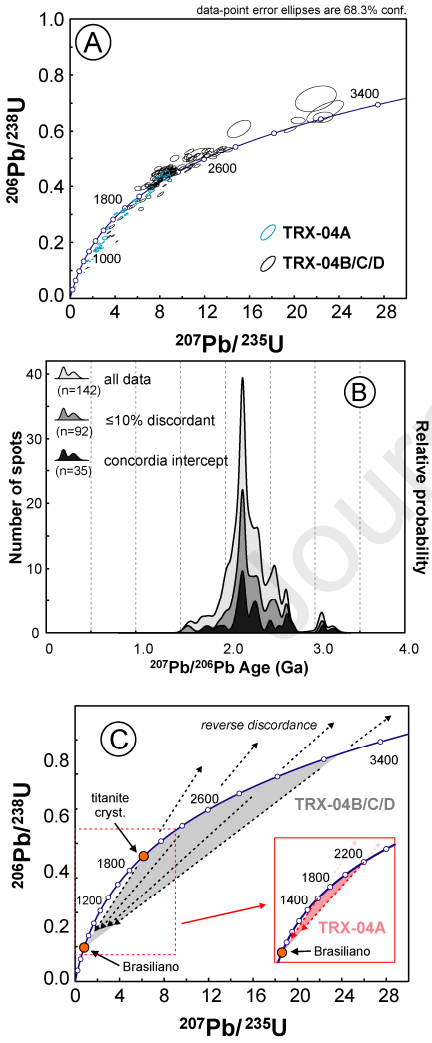

Figure 7: U-Pb zircon dataset for all spot analyses. The Concordia diagrams (A) shows the dataset comparing sample A (blue ellipses) with the other samples (black ellipses). (B) Shows probability density plots according to their respective $^{207}Pb/^{206}Pb$ ages; the dataset is separated into three categories: spot analyses that intersect the Concordia line within uncertainties, analyses ≤10% discordant and analyses >10% discordant. (C): schematic diagram on a Concordia diagram representing how a Neoproterozoic Pb redistribution event on samples recording a wide range of geological ages can produce a distribution of results similar to that observed in the dataset

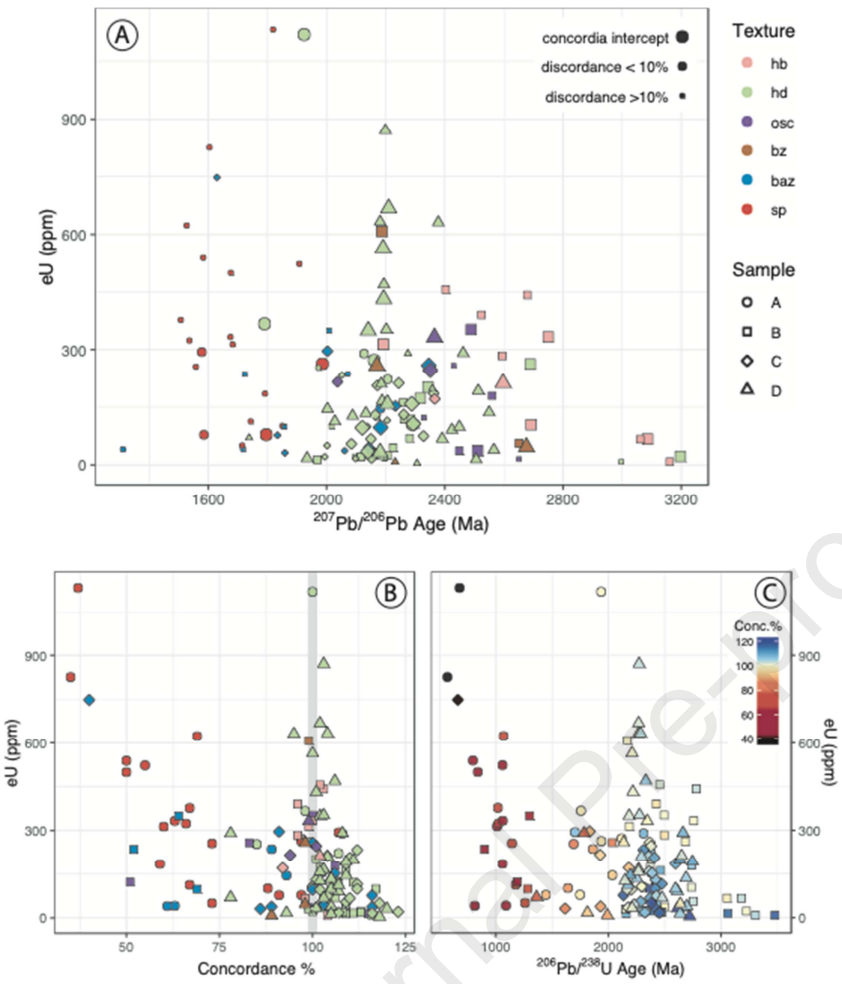

Figure 8: Relationships of U-Pb ages with effective Uranium (eU=U + 0.235*Th) . (A) shows the $^{207}Pb/^{206}$ Pb ages versus eU. Colors indicate the textures (hb: homogeneous bright, hd: homogeneous dark, osc: oscillatory zoning, bz: broad zoning, baz: broad altered zoning, sp: spongy/pourous) of the analysed spots, the shapes are according to the samples and symbol sizes indicates the degree of concordance. While hb texture is common in very old grains, most young and discordant ages have altered textures (sp and baz).(B) shows the eU content versus the degree of concordance, colors and shapes are as in A. Most highly normal discordant data (<100% Conc) occurs in grains with alteration textures and concordance correlates negatively with eU. Reverse discordance (>100%) is common in homogeneous dark grains and equally related with eU. (C) shows $^{206}Pb/^{238}U$ ages versus eU, shapes are as in A, color is according to concordance. For highly normal discordant data eU is negatively correlated with the $^{206}Pb/^{238}U$ age. For the sake of visibility two grains with eU>2000 ppm, U-Pb ages of ~1.4 Ga and concordance of ~20% are not displayed in A, B and C.

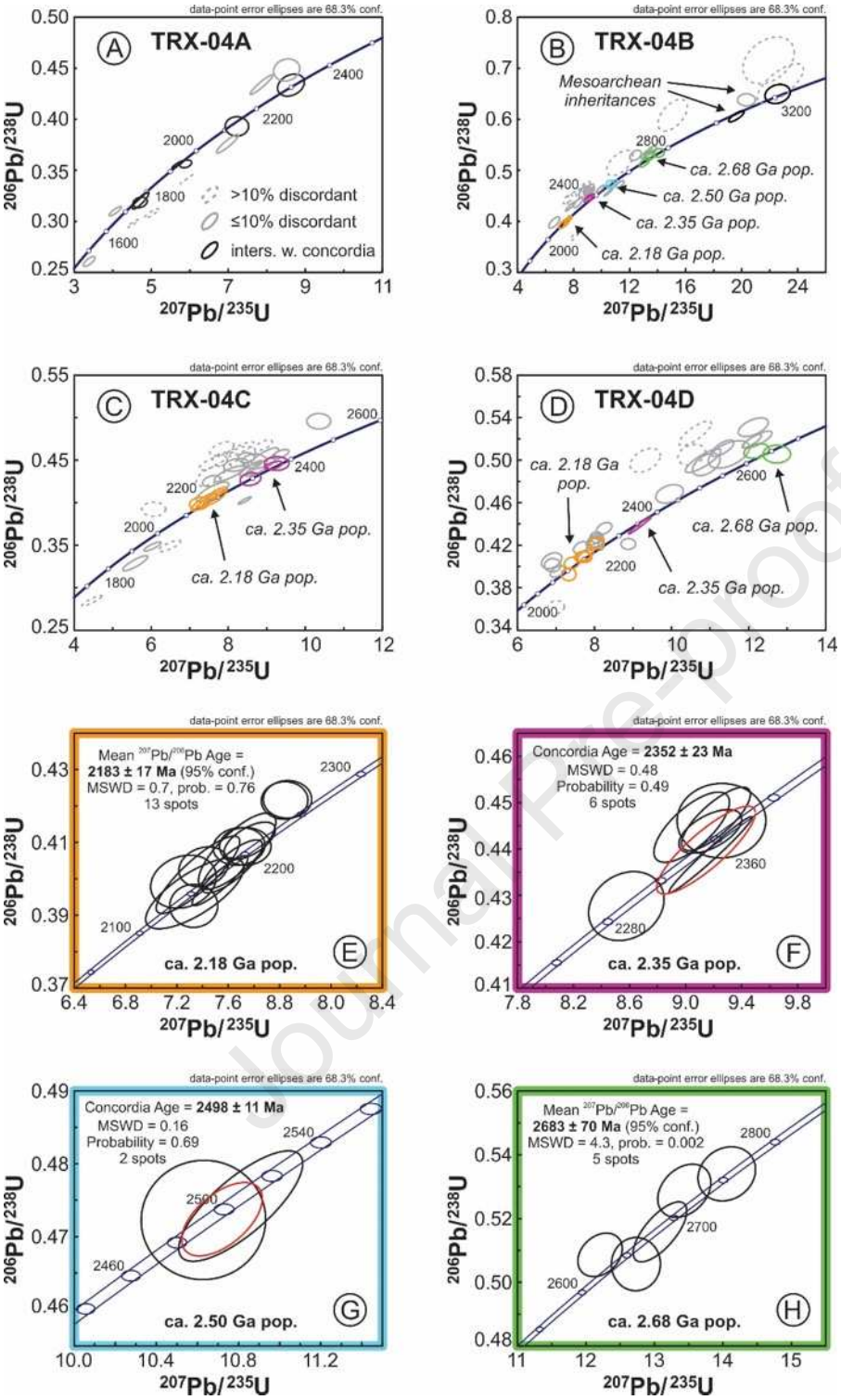

Figure 9: Concordia diagrams highlighting the most concordant U-Pb zircon results for each sample and main geological events. A-D: Samples TRX-04A, 04B, 04C and 04D. E-H: Calculated ages for the main populations observed in samples TRX-04B, 04C and 04D. In diagrams B-D the crystals used for age calculations are color-coded according to the main age populations, and the dataset is represented according to their degree of concordance following the legend in diagram A. Diagrams F-G only represent ellipses that intersect the Concordia line and calculated Concordia ages (red ellipse).

1127

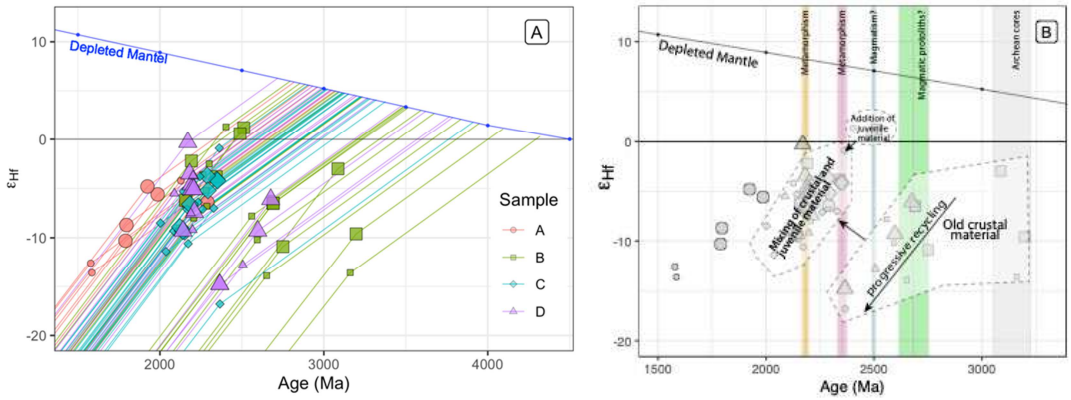

1128

1129 Figure 10: Representations of the Hafnium data of samples TRX – 04 A-D. (A): εHf(t1) values as a function of
1130 time for the four samples (TRX-04A: red circles, TRX-04B: green squares, TRX-04C: blue diamond, TRX-04D:
1131 purple triangles). Big symbols correspond to concordant analyses with U-Pb ages intercepting the Concordia
1132 curve, small symbols correspond to analyses up to 10% discordant. εHf(t1) is calculated from the measured
1133 $^{176/177}$ Hf isotope ratio and the corresponding U-Pb age. The paths indicate the evolution of εHf as a function of
1134 time. The intercepts of these paths with the εHf composition of the depleted mantel (blue line and dots)
1135 indicate the Depleted Mantle model age T_{DM}. (B) shows the same data as A emphasizing the main zircon
1136 populations (vertical colored bars, colors and ages are as in Figure 9) and the proposed differentiation and
1137 mixing processes interpreted for the dataset. Symbols and sizes are as in (A).

1138

- Concordant Zr U-Pb ranging from 3.2 -1.8 Ga represent complex evolution of the LAT
- Titanite crystallized at ≈2.0 Ga during a retrograde metamorphic trajectory
- Reverse discordant data indicate hydrothermal alteration during Neoproterozoic
- Hf-isotopes in zircon and titanite U-Pb ages seem to be unaffected by alteration

Author statement:

Beatrix M.Heller: Investigation, Writing-Original draft, Visualization
Mathias Hueck: Writing-Original draft, Visualization
Claudia R. Passarelli: Writing – Review and Editing
Miguel A.S. Basei: Supervision

Declaration of interests

☒ The authors declare that they have no known competing financial interests or personal relationships that could have appeared to influence the work reported in this paper.

☐The authors declare the following financial interests/personal relationships which may be considered as potential competing interests: